PIER M

(Received 31 January 2024, Accepted 25 March 2024, Scheduled April 1 2024)

Lasers Based on Periodic and Quasiperiodic Planar Feedback Cavities: Designs, Principle, and Potential Applications

Anwer Hayat[1], Alamgir[2], Yi Jin[1], Naeem Iqbal[3], Tianrui Zhai[3], and Sailing He[1,*]

[1]*National Engineering Research Center for Optical Instruments*
College of Optical Science and Engineering, Zhejiang University, Hangzhou 310058, China
[2]*School of Materials Science and Engineering, Zhejiang Sci-Tech University, Hangzhou 310018, China*
[3]*Faculty of Science, School of Physics and Optoelectronic Engineering, Beijing University of Technology, Beijing 100124, China*

ABSTRACT: Planar feedback micro-nanoscale cavities, shaped by advances in nanofabrication, have revolutionized laser technology, giving rise to chip-scale, low-threshold lasers with wide-ranging applications, spanning from atmospheric investigation to incorporation into central devices such as smartphones and computer chips. The complicated designs of these cavities, shaped by the physics of periodic and quasiperiodic structures, empower efficient manipulation of light-matter interaction and coherent light coupling, minimizing losses. This review thoroughly explores the underlying concepts and crucial parameters of planar feedback microcavities, shedding light on the photophysical behavior of recent gain materials pivotal for realizing optimal lasing properties. The examination extends to photonic crystal bandgap (PhC BG) microcavity lasers, specifically with periodic and quasiperiodic architectures. In-depth assessments probe into the principles and designs of each architecture, exploring features such as wavelength selectivity, tuneability, lasing patterns, and the narrow linewidth characteristics inherent in distributed feedback (DFB) microcavity lasers. The review highlights the intriguing characteristics of non-radiative bound states in the continuum (BIC) within periodic architectures, emphasizing trends toward high-quality factors, low thresholds, and directional and vortex beam lasing. It also explores the nascent field of Quasiperiodic (QP) microcavity lasers, addressing challenges related to disorder in traditional periodic structures. Comparative inquiries offer insights into the strengths and limitations of each architecture, while discussions on challenges and future directions aim to inspire innovation and collaboration in this dynamic field.

1. INTRODUCTION

Laser technology, rooted in Albert Einstein's discovery of stimulated emission, provides notable advantages such as high power and precise directionality. These qualities are essential for everyday use and show potential for advancements in spectroscopy, optical communication, and biomedical technologies [1–11]. Since Theodor Maiman's 1960 demonstration of the ruby laser, laser technology has led to key innovations, including the use of Rhodamine 6G in solid-state dye lasers and the discovery of laser activity in anthracene-doped fluorene single crystals emitting violet light [12–15]. In laser systems, three core elements are integral: the pumping assembly, which initiates lasing; stimulated emission through luminescent materials; and light confinement via the feedback cavity. Scientific studies highlights that the micro-nanoscale feedback cavity specifies a particular wavelength range within luminescent materials' photoluminescence (PL), tailoring emission characteristics including spatial, temporal, and power aspects [16–20]. Exploration of micro-nanoscale planar feedback cavities elucidates high-quality (Q) factors and small mode volumes, enriching light-matter interactions and resulting in efficient energy transfer, prolonged lifetimes, and reduced thresholds [21, 22]. These remarkable features find application across diverse scientific domains, including optical communications, integrated optics, sensors, and cavity quantum electrodynamics [23–26].

Research on microscale lasers was initiated in the 1980s within GaInAs quantum wells having dimensions close to several lasing wavelengths [27]. Since then, researchers have explored various micro-nanoscale cavities, including Fabry-Perot microcavity (F-P), distributed feedback (DFB), distributed Bragg reflection (DBR) microcavity, whispering gallery mode (WGM) cavities, and random cavities (RC) [17, 28–33]. In contrast to traditional laser systems, micro-nanoscale scattering structures maintain the feedback mechanism and significantly improve transverse mode or polarization state, wavelength selectivity, and resonator loss management by exchanging components [17, 19, 20, 34]. Prior research has examined microscale photonic crystals (PhCs), which employ a combination of dielectric and plasmonic structures to confine the electromagnetic density of states within a specific wavelength range termed the photonic bandgap (PBG) [35]. This ground-breaking discovery has unveiled new possibilities for manipulating electromagnetic wave physics by controlling optical mode density, especially at the photonic band edge (PBE), through adjustments in the periodicity and lattice structures of materials exhibiting PBG properties [17, 36–39]. As a result, these achievements have enabled Painter et al. to develop the first nanoscale laser based

* Corresponding author: Sailing He (sailing@jorcep.org).

on PhCs [40]. Soon after, two main types emerged: PBG defect mode and PBE lasers [41–44]. The former used the defect as a lasing cavity for lasing enhancement, while later, exhibits lasing action through the cavity, lacking defects that attain optical density of state at the PhC band edge. The PBE microcavity lasers maintain high gain and minimal propagation losses due to slow group velocity near PBE, which are critical for achieving a low threshold [44, 45]. Further, PBE lasers can be classified into two groups. The first involves guided modes linked to PBG within the crystal, which function as a lasing cavity. In contrast, the second relies on the waveguided (WG) modes determined by a combination of waveguide and PhC with weak modulation. In the latter, microcavity lasers include subwavelength gratings (1D and 2D) and waveguides, where the dispersion relation determines PBE laser features [46, 47]. Researchers have identified diverse PBG microcavity lasers featuring configurations such as distributed feedback (DFB), Bound State in Continuum (BICs), quasiperiodic structures (QPs), moiré patterns, and superlattices. Each setup employs distinct micro-nanoscale structures and principles to engineer lasing characteristics beyond the capabilities of traditional lasers. DFB lasers utilize 1D and 2D periodic grating structures to confine light within a specific range called the photonic bandgap, relying on diffraction, coupled wave, and PBG theories [48]. BIC lasers also employ periodic structures. However, their resonant frequency mode exists within the continuum spectrum, where light leaks out due to symmetry-protected or destructive interference states inside the planar feedback cavity [49]. Quasiperiodic structures depart from periodic arrangements, presenting increased diffraction peaks and forming continuous spectra in large samples. Emission wavelength and lasing patterns align with discrete sets of diffracted plane waves originating from reciprocal lattice points that meet the standing wave condition [50].

This review paper explores three main planar feedback cavity laser designs: DFB, BICs, and QPs, each with unique advantages and challenges in micro-nanoscale laser research. It covers micro-nanoscale cavity fundamentals, analyzes the photophysical behavior of various luminescent materials, and investigates recent advancements and optimization strategies for DFB architectures. Additionally, it discusses the potential of achieving BICs in periodic cavities, highlighting breakthroughs in low-threshold, directional emissions, and vortex beam outputs. The discussion extends to QPs planar feedback cavity lasers, addressing disorder-related issues in traditional periodic structures and emphasizing their potential for tailored spectral properties and enhanced robustness.

2. FUNDAMENTALS FOR MICRO-NANOSCALE CAVITY LASERS

The miniaturization of semiconductor lasers to the micro-nanoscale has been a subject of research for years, but has met some challenges due to high losses. This has impeded the development of high-density Photonic Integrated Circuits (PICs) [51]. However, recent advancements in nanocavity physics are showing great promise in producing long-lasting, spatially confined resonances while enabling precise control over far-field radiation [52]. GaInAs quantum wells were used in the 1980s to fabricate microlasers with dimensions of the building blocks that matched several lasing wavelengths [27]. Since then, researchers have been exploring alternative optical materials at the wavelength scale to progress in the development of similar microlasers. Although there are many possible applications for microlasers, there are certain inherent challenges due to their mechanical stiffness, high processing costs, and limited tunability. Therefore, exploring alternative approaches to overcome these drawbacks is necessary. As discussed in the introduction every laser includes three basic components: cavity, material, and pump source. The following section will provide a summary of each of them.

2.1. Generalities and Features Parameters of Micro-Nanoscale Feedback Cavities

Optical micro-nanoscale cavities have always been an essential element of lasers since their inception. They significantly enhance photon-material interactions and provide indispensable optical feedback. Optical microcavities function as resonators, confining light to diminutive volumes through resonant recirculation, typically at or below the wavelength of light. There are three highly efficient effective methodologies for light confinement in micro-nanoscale microcavities [17, 53]. The first strategy involves incorporating a gain medium positioned between two mirrors, which can be metallic or dielectric multilayers called DBR. The Fabry-Perot (FP) structure is a prevalent microcavity design that utilizes two closely spaced flat mirrors engineered to accommodate a restricted range of light wavelengths, typically tailored to match integer multiples of half-wavelength values (Fig. 1(a)) [54–56]. The second strategy, WGM microcavity, creates a total reflection interface between a high refractive index inside and a low refractive index outside, limiting light propagation (Fig. 1(b)) [57]. The third strategy uses microstructures patterned on the resonant optical wavelength scale (grating) and the photonic crystal, capable of confining light within specific frequency ranges (Fig. 1(c)) [58–60]. Photonic crystals exist in 2D and 3D configurations, with radiation loss predominantly occurring in 1D and 2D photonic crystals [17]. Theoretically, the 3D case demonstrates minimized radiation loss due to a 3D photonic bandgap, facilitating effective three-dimensional light confinement [61–63].

To attain peak performance in micro-nanoscale cavity configurations, it is vital to employ diverse light-confinement strategies, directly influencing essential features of the oscillating laser light field. Among these features, the resonant wavelengths (frequencies) allowed by the gain medium's emission spectrum hold particular significance. This relationship can be expressed mathematically by connecting the round-trip optical path (R) and the resonant wavelength (λ), where "m" is an integer: $R = m\lambda/2$. The discretization of resonant wavelengths results from the boundary conditions placed on the confined photons within the cavity, which demand a consistent phase throughout a round-trip propagation. This requirement significantly influences various characteristics that depend on the cavity properties. These configurations define the spatial attributes characterizing the laser beam emitted from the res-

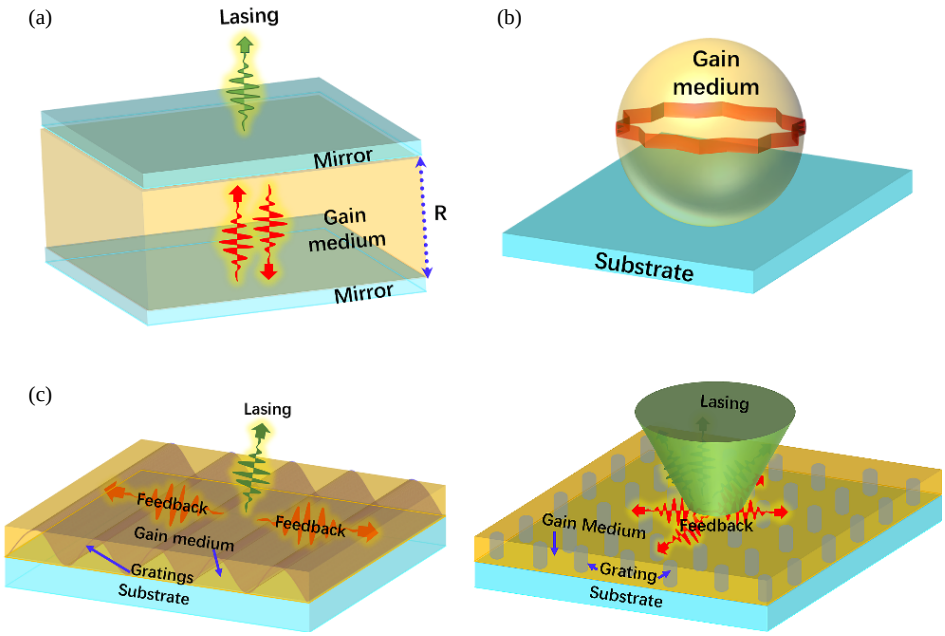

FIGURE 1. Optical micro-nanoscale cavity designs: varied strategies for trapping and sustaining light in confined spaces. (a) Conventional FP microcavity confines light through reflection. (b) WGM microcavity employs total internal reflection in a circular ring with a difference between high and low index. (c) DFB microcavity achieves light confinement via wavelength-scale structural scattering.

onator. One must ensure that the permissible resonant frequencies of the laser align with the gain material's photoluminescence (PL) spectrum. The gain must equal or surpass the losses incurred during a single round-trip within the cavity for stable oscillation of the laser mode. Meticulous cavity design is required to achieve lasing, ensuring congruence between the material's mode and gain spectra. In principle, microcavities play a critical role in shaping lasers' frequency, spatial properties, and power dynamics. The cavity's longitudinal or axial modes and linewidth govern the frequency, while spatial attributes encompass the laser's pattern, polarization, and beam divergence. Power characteristics, including the laser threshold and output efficiency, are also considerations. The critical determinants of microcavities encompass their type, material, quality, and dimensions [16–18, 64–66].

To gain a comprehensive understanding of micro-nanoscale cavity designs, we compare their diverse optical properties. Such an approach allows us to comprehend these designs and their potential applications better [22]. The performance of micro-nanoscale cavity lasers depends on the Q factor, which measures the damping of resonator modes, evaluates the magnitude of loss within the microcavity, and assesses the mode volume, which describes the spatial limitations that the microcavity sets for photons. It is defined simply as the quotient of the resonant cavity wavelength (λ_c) divided by the linewidth (FWHM) of the cavity mode ($\Delta\lambda_c$): $\lambda_c/\Delta\lambda_c$. The Q-factor of a cavity holds significant importance in influencing various laser attributes. These encompass the laser linewidth, dictating the spectral coherence and monochromaticity of the laser emission; photon lifetime, denoting the duration for the resonator cavity's energy to decay to $1/e$ of its initial value; and the lasing threshold, representing the minimum optical pump power required for stimulated emission generation. Another crucial parameter for resonators is finesse, calculated as the ratio of the free spectral range (the frequency separation between successive longitudinal cavity modes, $\delta\lambda_c$) to the linewidth (FWHM) of the resonances; $F = \delta\lambda_c/\Delta\lambda_c$. The interval between longitudinal modes in a microcavity decreases as the cavity length increases. Non-confocal cavities exhibit transverse optical modes at varied frequencies, and their scaling follows a similar pattern to the cavity length [67, 68].

Microcavities possess fewer optical modes within each spectral region than macroscopic cavities. This suggests that fine-tuning the cavity mode to a specific emission wavelength becomes more critical in micro-nanoscale cavities than larger cavities. Microcavities are smaller than macroscopic cavities in all three spatial directions, making their angular emission patterns broader. This means that microcavities emit across a larger solid angle when they are in resonance. However, they still have directional beaming in specific directions despite the broader angular emission. Microcavities can achieve lower lasing thresholds due to two primary factors: a smaller number of optical modes and a reduced gain volume. Within a microcavity, an embedded emitter (gain medium) experiences a narrower range of optical states for potential emission. In contrast to free space where emission can occur across any solid angle and frequency, the microcavity serves to organize the optical density of states surrounding the emitter.

2.2. Gain Medium

Laser technology has undergone a significant transformation with the emergence of the gain medium, which plays a crucial role in enhancing the intensity of incoming light through

stimulated emission. This process produces a second photon that shares the same phase and frequency with the stimulating photon. The development of micro-nanoscale cavity lasers has opened up a world of possibilities using diverse materials in various forms and combinations, allowing for emissions across a broad spectrum of wavelengths, from ultraviolet to infrared [20, 69–72].

While traditional high-performance lasers have been limited in their use of luminescent materials, including inorganic semiconductors and doped crystals, which often originate with inherent limitations such as brittleness and inflexibility, recent advancements in organic semiconductor materials offer a more straightforward processing approach [73–76]. Devices produced from such materials can be mechanically manipulated easily, and they have demonstrated remarkable biocompatibility, making them an attractive option for various applications.

Integrating quantum dots and perovskites into lasers has further expanded the scope of materials for researchers and scientists to explore [77–79]. Organic semiconductors, organic dyes, and semiconductor quantum dots, allow for even better and more efficient laser devices. The distinct features of materials, including their capacity for film formation, conductivity, and manufacturing complexities, present potential avenues for creative exploration and experimentation.

2.2.1. Organic Semiconductors and Dyes

Although organic semiconductors and laser dyes both exhibit broad spectra and tunability across the visible spectrum, organic semiconductors have certain advantages. These materials can achieve high photoluminescence quantum yield (PLQY) even in neat solid-state films, offering superior pump absorption and gain without significant dilution. Furthermore, the simplicity of processing, such as solution processing, is a characteristic advantage of many organic semiconductors, potentially enabling the creation of thin-film laser structures. The charge transport capability of organic semiconductor films opens avenues for electrical pumping [16, 53, 70].

Organic semiconductors relevant to lasing are extended molecules with randomly oriented chromophores, unveiling photophysical properties through molecular orbital overlap evident in time-resolved spectroscopy. While initial investigations focused on light-emitting single crystals like anthracene, challenges in growth and handling led to Tang and Van Slyke's breakthrough in efficient electroluminescence found in evaporated films of small molecule organic semiconductors, illustrated by aluminum tris(quinolate), sparking considerable interest in their light emission applications [15, 80]. Additionally, three other organic semiconductor types have been explored for lasers: conjugated polymers, marked by long chain-like molecules like poly(phenylenevinylene)s, ladder-type poly(para-phenylene), and polyfluorenes; conjugated dendrimers display a highly branched structure with a chromophore core and conjugated branches; and spiro-compounds, comprising two oligomers accompanying by a spiro linkage [81–86].

Organic semiconductors exhibit robust light absorption and effective luminescence characteristics, boasting a typical absorption cross-section value of $10^{-16}\,\mathrm{cm}^2$. This attribute enables 90% light absorption within a film thickness of approximately 100 nm, facilitating low pumping fluences in films and achieving high optical gain [81]. Efforts have been made to increase the PLQE of organic semiconductor thin films by tailoring the PL spectra through modification of conjunction length or installing electron-acceptor/donor group, localizing excitons, and minimizing intermolecular interactions, all of which are important for achieving high gain and low-threshold organic lasers [88, 89]. The photophysical behavior of organic semiconductors mimics a four-level laser system, where incident photon absorption drives an electron from lower band (Level 1, S_0) to higher electronic band (Level 2, S_n) before rapidly internalizing to the lowest electronic excited band (Level 3, S_1) vibrational manifold within a sub-picosecond timeframe. This rapid relaxation, facilitated by the close spacing of vibronic sublevels, promotes efficient population inversion between the lowest vibrational level of S_1 (Level 3) and the higher unoccupied vibrational levels of the S_0 (Level 4) manifold, following the transition toward ground-state via thermalization, enabling laser action at remarkably low pumping rates. Singlet excited states enhance optical gain, but triplets and polarons pose challenges to lasing in organic devices (Fig. 2(a)). The long decay lifetimes and broad absorption spectra of triplets, formed via intersystem crossing, and polarons, arising from charge localization, impede optical enhancement, mainly when distributed across distinct molecular chains, as shown in Fig. 2(a) [53]. Initial observations of lasing occurred in a film of the conjugated polymer poly (p-phenylene vinylene), PPV [90]. Subsequent research explored various polymers for microcavity lasers spanning the entire visible spectrum, including poly[9,9-dioctylfluorenyl-2,7-diyl]-end-capped with DMP (PFO, American Dye Source), poly[(9,9-dioctylfluorenyl-2,7-diyl)-alt-co-(1,4-benzo-(2,1′,3)-thiadiazole)] (F8BT, American Dye Source), and poly[2-methoxy-5-(3′,7′-dimethyloctyloxy)-1,4-phenylenevinylene] (MDMO-PPV, Sigma-Aldrich) [90–92]. The absorption and PL spectra of PFO, F8BT, and MDMO-PPV highlight significant Stokes shifts, effectively preventing the absorption of emitted light (Figs. 2(b)–2(d)) [87].

In the evolution of laser technology, organic laser dyes have played a pivotal role owing to their exceptional characteristics. These materials exhibit strong absorptions, broad spectra, outstanding tunability, and ease of fabrication, resulting in spectral narrowing under specific conditions. Despite their advantageous features, the non-conductive nature of organic dyes presents a hurdle in the development of electrically pumped laser devices. Notably, cyanine, oxazine, coumarin, and rhodamine are significant dye categories that offer controllable laser wavelength, high fluorescence efficiency, low laser threshold, and cost-effectiveness — however, their susceptibility to easy bleaching challenges the stability of laser emission [16–18, 64, 70].

2.2.2. Colloidal Quantum Dots (CQDs)

CQDs, typically measuring only a few nanometers in size, demonstrate a fascinating phenomenon known as quantum con-

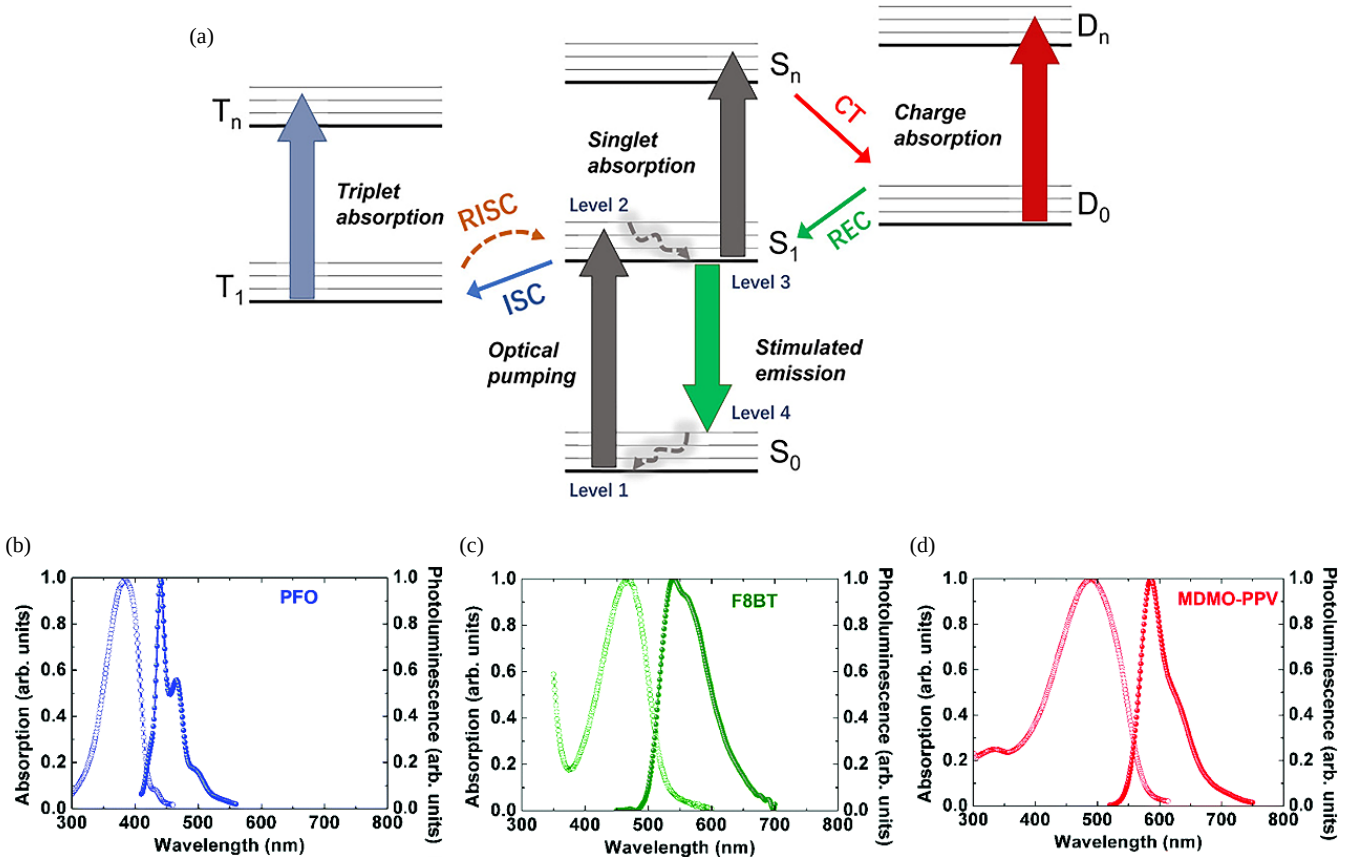

FIGURE 2. Schematic for photophysical behavior of organic semiconductors through singlets, triplets, and charge states. The absorption and photoluminescent spectra of three gain mediums. (a) The 4-level system (level label with 1–4) for attaining lasing along with the key progressions of ISC, RISC, CT, and REC. ISC refers to intersystem crossing, RISC denotes reverse intersystem crossing, CT stands for charge separation, and REC represents carrier recombination. Absorption (blue, green and red dotted line) and photoluminescence (blue, green and red solid line) spectrum of; (b) PFO, (c) F8BT and (d) MDMO-PPV [53, 87].

finement. This implies that their material properties are directly influenced by their dimension when all three dimensions are comparable to or less than the exciton Bohr radius of the original bulk solid, as shown in Fig. 3(a). The successful lasing action of CdSe colloidal quantum dots (CQDs) within a Fabry-Pérot cavity in glass samples, reported in 1991, acknowledged the substantial potential of semiconductor quantum dots as gain materials for laser applications [93]. The recent research on CQDs has resulted in significant advancements in manipulating their optical gain properties. One recent study proposed a strategy for controlling the photoluminescence emission of AlQDs by manipulating surfactants and phosphonic acids on their surface, revealing that competitive binding of these ligands affects the emission properties [94]. Researchers have achieved low-threshold, sub-single-exciton lasing by controlling their composition to inhibit nonradiative Auger decay and using photochemical charging to reduce ground-state absorption [95, 96]. These breakthroughs have opened the door to realizing optical gain through direct current (D.C.) electrical injection and practical implementation of dual-function devices that can serve as both a standard LED and an optically pumped laser [97, 98]. These notable developments have brought researchers closer to achieving the longstanding goal of creating electrically pumped lasing devices with CQDs. A comprehensive analysis of the optical gain and lasing characteristics of CQDs has been extensively documented in reviews dedicated to this specific topic and broader discussions covering colloidal nanostructures [99, 100].

To comprehend the photophysical behavior within tightly confined CQDs, a constructive approach involves simplifying the analysis of the lowest-energy emitting transition to a two-level scheme characterized by two electrons with opposite spins residing in the valence band (VB), as depicted in the left section of Fig. 3(b), absorption. Although this scenario permits light emission, it fails to amplify incident photons due to the equal likelihood of stimulated emission by the conduction band (CB) electron and photon absorption by the VB electron, termed 'optical transparency' or the optical gain threshold, as shown in the middle section of Fig. 3(b). However, CQD light amplification ensues only when the second VB electron is excited to the CB, implying that the population inversion necessary for lasing action occurs when a fraction of the CQDs in the sample is excited with two electron-hole pairs or biexcitons as seen in the right section of Fig. 3(b) [18, 20, 100]. Quantum dots, particularly III-V and II-VI (CQDs), are becoming increasingly popular in laser applications. III-V CQDs are created on a semiconductor

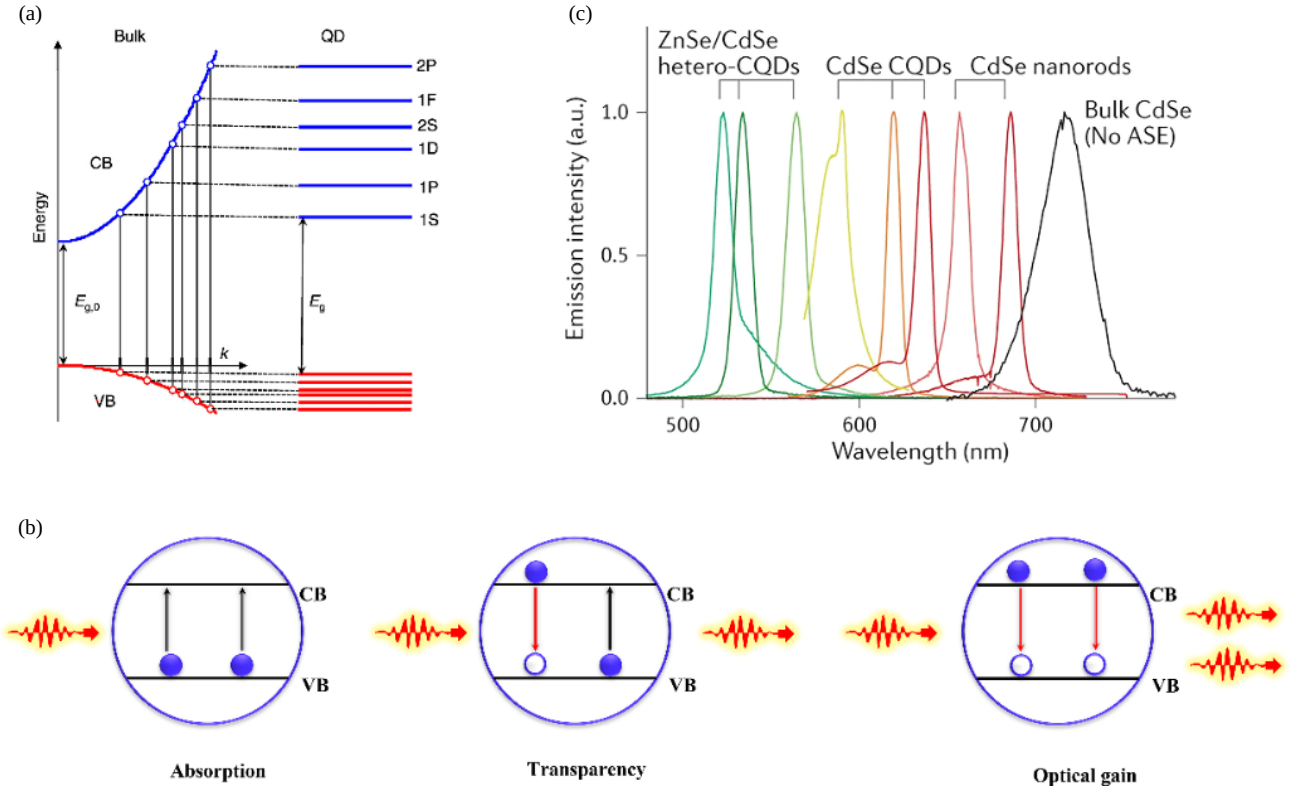

FIGURE 3. Shows a schematic of CQDs for the emergence of energy levels, photophysical behavior, and emission properties spectra of CQDs. (a) Comparison of the bandgap of bulk semiconductors with continuous valance and conduction bands to the discrete energy levels of CQDs, which are related to the quantum confinement effect. (b) A two-level system in CQDs for the stimulated emission process, where the right section shows a biexciton state (optical gain). (c) The amplified spontaneous emission (ASE) spectra of CdSe CQDs with various morphologies covering the most visible spectrum [101, 102].

substrate, while II-VI CQDs are integrated into transparent dielectric matrices [20]. These quantum dots allow for customizable emissions in various colors, bridging the gaps in the current color space beyond the capabilities of existing semiconductor laser diodes. Experiments have shown that II-VI CQDs can amplify light across the visible spectrum, as CdSe-based CQDs exhibit multicolor amplified spontaneous emission ranging from 690 nm (red) to 520 nm (green), as shown in Fig. 3(c) [101].

2.2.3. Perovskite

Perovskite materials have captivated the realm of laser technology since their discovery in 1998, initially demonstrating ability under low-temperature circumstances [103]. In 2014, researchers successfully achieved perovskite lasers operating at room temperature [104]. Scientists have embarked on an exploration of diverse perovskite variants, ranging from quantum dots and nanowires to nanoplates and 3D films, all with the overarching goal of achieving low-threshold lasing or amplified spontaneous emission [69, 105–107].

Within the perovskite family, two crystalline structures, namely AMX_3 and A_2MX_4, have emerged, prompting intensive investigations into their properties. These compounds feature a nuanced composition, encompassing cations A (both inorganic and organic types like Cs^+, formamidinium (FA^+), methylammonium (MA^+)), divalent metallic cations M (Pb^{2+}, Sn^{2+}, Mn^{2+}, Fe^{2+}), and halogen anions X (I^-, Br^-, Cl^-). The band-edge (BE) electronic states in lead halide perovskites predominantly arise from $[PbX_6]^{4+}$ octahedra. Altering the halide element, from iodine to chlorine, induces a reduction in lattice parameters, fostering increased orbital overlap and consequent widening of the bandgap. This emission wavelength adaptability throughout the visible spectrum is readily attainable by adjusting stoichiometry through halide substitution or by exchanging organic components with alternatives like Cs, providing avenues for extension into the ultraviolet or near-infrared spectral domains (Fig. 4(c)) [105]. The versatility of $CsPbX_3$ quantum dots within this perovskite family is underscored by their high quantum yield of $\approx 90\%$ and the ability to tune bandgaps from 400–710 nm, even without surface passivation [108]. Analogous to inorganic semiconductors, perovskites' optical properties are governed by excitons-bound electron-hole pairs — whose binding energies (E_b) dictate stability concerning temperature fluctuations [69].

Perovskites exhibit the capability to enhance incoming photons through stimulated emission, despite encountering challenges like nonradiative pathways, scattering media, and photon reabsorption. The photophysical mechanism unfolds rapidly upon photon excitation, generating electron-hole pairs within tens of femtoseconds. These hot carriers promptly cool down through lattice interactions, releasing excess energy through optical and acoustical phonon emission [69, 106].

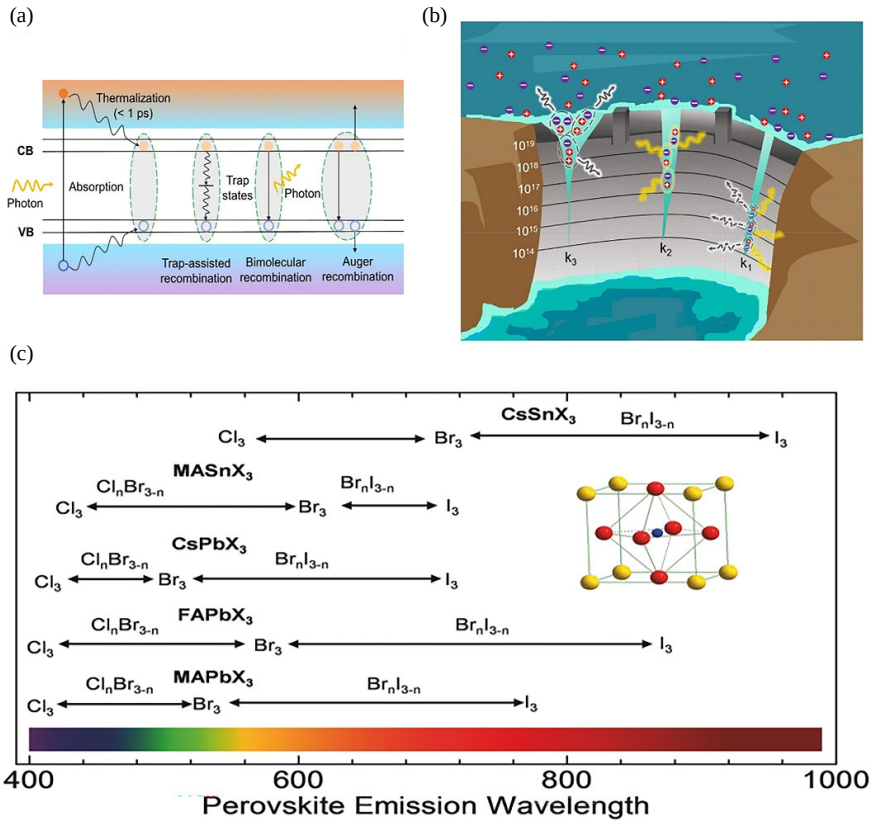

FIGURE 4. Perovskite photophysical mechanism and band gap engineering: Schematic depicts, (a) stimulated emission mechanism in perovskites involving bimolecular recombination with non-radiative channels such as trap-assisted and Auger recombination. (b) The picture show that the electron-hole recombination is analogous to water falling from dams, illustrating different channel flows correlating to charge-carrying densities. Yellow and gray wave arrows indicate the recombination processes of radiative (k_2, bimolecular) and non-radiative (k_1 and k_3, trap-assisted and Auger). (c) Band gap engineering plots obtained through stoichiometry or exchanging organic components to enhance emission spectra across the electromagnetic spectrum [105, 106].

Recombination of charge carriers near the band edge ensues through various channels, including trap-assisted, bimolecular, and Auger recombination (Fig. 4(a)). Zhao and collaborators have illustrated these recombination channels through a captivating analogy: a river flowing through a dam. The water level symbolizes carrier density, with the diagram elucidating three recombination channels exhibiting distinct behaviors across various charge carrier density regimes. The diagram introduces three crucial recombination coefficients — k_1 (monomolecular), k_2 (bimolecular), and k_3 (three-body Auger) — each playing a pivotal role in the intricate process of recombination (Fig. 4(b)) [106]. Below a charge carrier density of $10^{15}\,\mathrm{cm}^{-3}$, the monomolecular recombination mechanism dominates, involving trap-assisted nonradiative or radiative exciton recombination [109, 110]. As carrier densities exceed $10^{16}\,\mathrm{cm}^{-3}$, the recombination mechanism gradually shifts towards radiative bimolecular recombination, facilitated by charge carrier trapping. Serving as a direct bandgap gain medium, perovskites exhibits bimolecular recombination originating from radiative band-to-band transitions — a process akin to inverse absorption [111]. Auger recombination gains prominence as carrier densities approach the laser working regime ($> 10^{18}\,\mathrm{cm}^{-3}$), characterized by a three-body process transferring energy within excited electron-hole pairs [112].

Metal halide perovskites are promising materials due to their exceptional characteristics. These include a remarkable ability to absorb high levels of visible and near-infrared light, boasting absorption coefficients around 10^4–$10^5\,\mathrm{cm}^{-1}$. Tolerance for defects is enhanced by the presence of oxidized cations (Pb^{2+}) and the ionicity of perovskites, contributing to the creation of shallow defects near the band edge. This unique feature results in a high photoluminescence quantum yield (PLQY) of up to 90% for perovskite thin films and nanocrystals. Researchers have delved into the gain lifetime of halide perovskites, employing techniques such as time-resolved photoluminescence and transient absorption spectroscopy. The expansive range of compositions, dimensionalities, and ease of fabrication positions perovskite materials as exceptional candidates for laser development, promising significant strides in optoelectronics [69, 105, 106].

3. MICROCAVITY LASING IN PHOTONIC CRYSTALS

PhCs are wavelength-scale structural configurations capable of constraining light propagation within specific frequency ranges. The achievement of a complete photonic bandgap is dependent on the alignment of specific axes and a uniform variation in refractive index within the periodic or quasiperi-

odic structure. Inherent limitations exist within photonic crystal structures. Despite their display of robust Bragg scattering, they encounter Rayleigh scattering, introducing potential challenges like propagation loss and optical signal dephasing, contributing to the comprehension of speckles [35, 113].

The introduction of randomness in the positioning, dimensions, and shapes of elements within the photonic crystal structure can induce a spectrum of Rayleigh scattering effects. This variability creates opportunities for innovating new functionalities and applications in photonics. These periodic structures, arising from the multiple scattering of photons within a wavelength scale, can adopt diverse dimensions, including 1D, 2D, and 3D configurations. Customizing spatial structures in photonic crystals facilitates the design of various functionalities, illustrated by DFB cavities [17, 114, 115].

The theoretical ideal of a 3D photonic crystal microcavity involves a defect within a perfect 3D photonic lattice with a high refractive index contrast, leading to a bandgap at a specific wavelength in all directions [16]. However, the practical fabrication of such structures presents considerable challenges. Researchers are actively exploring unconventional lattice geometries like photonic quasicrystals and Moiré pattern lattices to overcome these hurdles and pioneer novel photonic materials with unparalleled properties. The interest in these periodic and unconventional lattice geometries stems from their potential to achieve diverse temporal, spatial, spectral, and power-related properties [116]. In this section, we will discuss the fundamental principles, designs, and recent advancements of the microcavity lasers, including DFB, BICs and QPs microcavity lasers.

3.1. Working Principle and Design of DFB

Within PhC micro-nanoscale cavity lasers, DFB resonators integrate diffractive structures on the wavelength scale to optimize the efficiency of light propagation. This structural arrangement entails the use of a gain waveguide aligned parallel to the sample plane, where the substrate or waveguide core incorporates a periodic corrugation promoting the scattering of guided modes for coherent recombination. Through meticulous alignment with specific wavelengths, this periodic modulation induces constructive interference, providing the necessary optical feedback for the initiation of lasing. Subsequent investigations involve a diverse range of theoretical, simulation, and analytical methods aimed at comprehending the fundamental physical principles that govern DFB microcavities. Notably, diffraction, coupled wave, and photonic bandgap theories provide top-down strategies for aligning the gain medium with microscale structures and customizing its emission characteristics.

Diffraction theory highlights the significance of the periodic patterns between the gain film and substrate in providing a vital feedback mechanism, facilitating an effective coupling of in-plane feedback light with the emitted output, and serving as a waveguide. Fig. 5(a) illustrates that when a specific corrugation period is applied, a distinctive set of wavelengths is diffracted from a propagating mode of the waveguide (red curve) into the counterpropagating waveguide mode (solid red arrow), which is given by Bragg condition:

$$\lambda_{\text{lasing}} = 2n_{eff}\Lambda \sin\theta/m \tag{1}$$

where λ_{lasing} is the emission wavelength, n_{eff} is the waveguide effective refractive index, Λ is the corrugation period, θ is the angle between the feedback light within the cavity and normal interface, and m represents positive integer maintaining the Brag condition due to feedback mechanism within the waveguide. The feedback within the plane of gratings can be attained by normal incidence ($\theta = 90$), the formula of the DFB takes the following form:

$$\lambda_{\text{lasing}} = 2n_{eff}\Lambda/m \tag{2}$$

The equation highlights a key measure for achieving DFB lasing. Resonance is established through m^{th}-order diffraction in an m^{th}-order DFB system ($m > 2$). Output coupling phenomena can manifest through various diffraction orders, specifically those with order numbers less than or equal to $|m|$. This can lead to observing multiple output directions during the laser's action, see the upper panels of Figs. 5(c), (d) and (e). The laser output emanating from the m^{th} Bragg order is called edge emission, with the output beam occurring at an angle of $\phi = \pi/2$. Additionally, emission from the 2$^{\text{nd}}$ and higher diffraction orders can give rise to surface emission lasing ($\phi = [0, \pi/2]$). The lower panels of Figs. 5(c)–(e) depict photographs of lasers patterns of the 2$^{\text{nd}}$, 3$^{\text{rd}}$ and 4$^{\text{th}}$ 1D DFB microcavity upon optical pumping. Therefore, it is imperative that the relationship between emitted radiation and diffraction order adheres to the conditions for constructive interference and is delineated by a mathematical correlation as follows:

$$\sin(\phi) = n_{eff}(2l/m - 1) \tag{3}$$

$\{\phi$ is the emitted radiation angle, l is an integer $= (0, m)\}$

The schematic representation of the above equation can be seen in Fig. 5(b). Where emitted radiation can make an angle (ϕ) with normal incident after satisfy the Bragg condition. The extension of diffraction theory allows for a more comprehensive understanding of the operational characteristics in higher-order DFB lasers, with potential applications in higher dimensions (2D or 3D), while specifically avoiding consideration of individual cavity coupling. Additionally, beyond diffraction theory, the determination of lasing modes, such as Transverse Electric (TE) or Transverse Magnetic (TM), is contingent upon the critical thickness of the active medium film, denoted as the critical thickness. In 2021, Chu et al. developed a 2$^{\text{nd}}$ order circular grating DFB laser utilizing a tactful spin-coating method to apply an ultra-thin film (~ 110 nm) of the conjugated polymer F8BT as the gain medium. By leveraging the critical thickness formula, they successfully achieved single-mode lasing at the zero-order TE mode, demonstrating a notably low threshold of approximately 19 μJ/cm^2 [117].

The theoretical framework that forms the basis of DFB lasers is incredibly intricate, exceeding the limitations of a fundamental diffractive model. The wavelength that meets the Bragg condition cannot propagate within the film, leading to the formation of a photonic stopband. Positioned at the Bragg wavelength, this stopband significantly modulates the directionality of light propagation orthogonal to the grating groove. Through the utilization of a 2D/3D grating coupled with vigorous feedback, the photonic stopband has the potential to evolve into a complete photonic band gap, impeding the propagation of

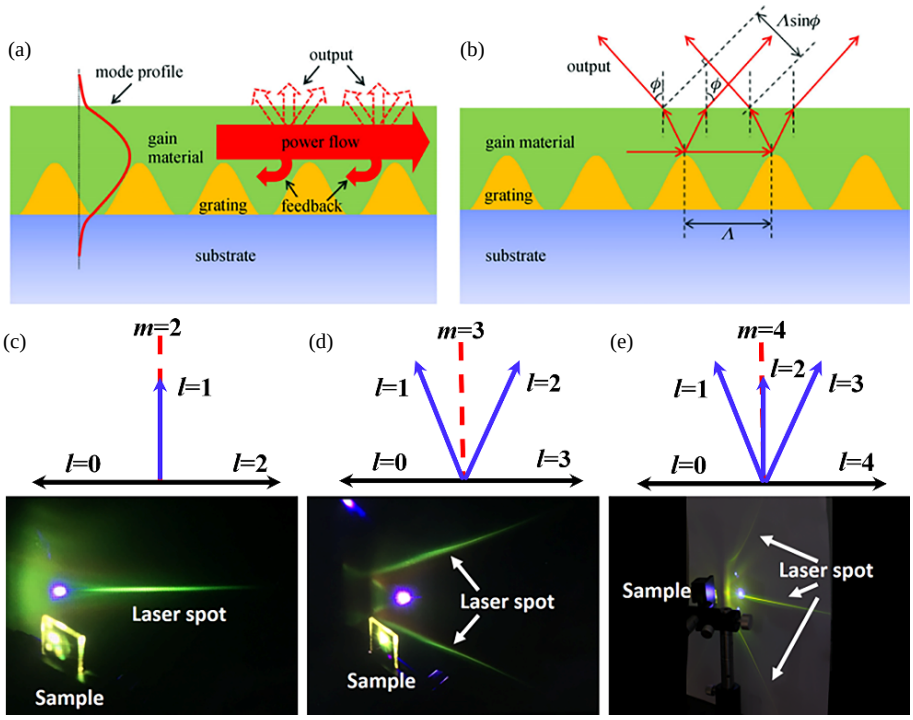

FIGURE 5. 1D DFB working principle based on diffraction model and lasing patterns: (a) Schematic of the interaction between the waveguide mode, counterpropagating, and output emission characteristic. (b) Ray optics satisfying constructive interference conditions for output emission properties of higher order DFB at various angles. The upper and low panels indicate the emission directions and operating lasing patterns in photographs, (c) 2nd, (d) 3rd, and (e) 4th order DFB cavity [59].

a spectrum of wavelengths in all directions. In general, DFB lasers operate with oscillations on a pair of wavelengths situated at either edge of this photonic stopband, as predicted by the coupled mode theory put forth by Kogelnik and Shank [118]. Despite using approximations, this theoretical framework proves advantageous in examining mode spatial distributions, emission wavelength, and effective refractive index. It elucidates the physical mechanisms that govern DFB lasers, encompassing resonant mode patterns, mode selectivity, discrepancy in quantum efficiency, threshold behavior, and the influence of boundary reflections [119, 120]. Researchers have developed an analytical model unifying waveguide and coupled-wave models to provide a more comprehensive and precise picture of the DFB cavity. The model considers diffraction and waveguide theories to determine the resonant wavelength [121]. The photonic bandgap model elucidates the physical mechanism of DFB lasers by stating that the resonant wavelength that meets the Bragg condition cannot exist within the cavity due to the photonic bandgap [122, 123]. Therefore, the solution to the 1D coupled wave theory, expressing the resonant wavelengths satisfying the Bragg condition in a dispersion relation, can be written as follows:

$$\kappa = \beta_B \pm \sqrt{\Delta\beta^2 - |\kappa|^2}, \quad \begin{pmatrix} \beta_B = \frac{mG}{2} \\ G = \frac{2\pi}{\Lambda} \\ \Delta\beta = \beta_z - \beta_B \\ \beta_z = \frac{2\pi n_{eff}}{\lambda_0} \end{pmatrix} \tag{4}$$

where the parameters in Eq. (4) κ, β_B, and β_z represent the coupling coefficient, grating wave vector, and the wave vector in the z-direction, respectively. The correlation between various resonant wavelengths and the Bragg condition exhibits promising characteristics, aligning with the photonic bandgap. This alignment suggests that the photonic bandgap theory has the potential to furnish a comprehensive physical picture of higher dimensions (2D and 3D) in DFB lasers. The augmented degree of freedom inherent in the photonic bandgap facilitates a more concentrated feedback behavior [124].

3.1.1. 1D DFB Planar Feedback Cavity Lasers

The exploration of 1D DFB planar feedback cavity lasers has been extensive, encompassing diverse materials like organic polymers, small molecules, inorganic semiconductors, colloidal quantum dots (CQDs), and perovskites, spanning the entire visible to infrared spectra [17, 20, 105]. Researchers have diligently incorporated various materials, such as spiro materials and energy transfer blends, to significantly reduce lasing thresholds [16, 18]. While the field has made notable progress, ongoing efforts focus on optimizing the design of 1D DFB micro-nanoscale cavities, exploring different grating types like regular, chirped, beat, and compound to enhance lasing performance [125–137].

The Literature studies the optimization of parameters such as grating diffraction order, period, and waveguide thickness to achieve tunability within the 20–50 nm lasing wavelength

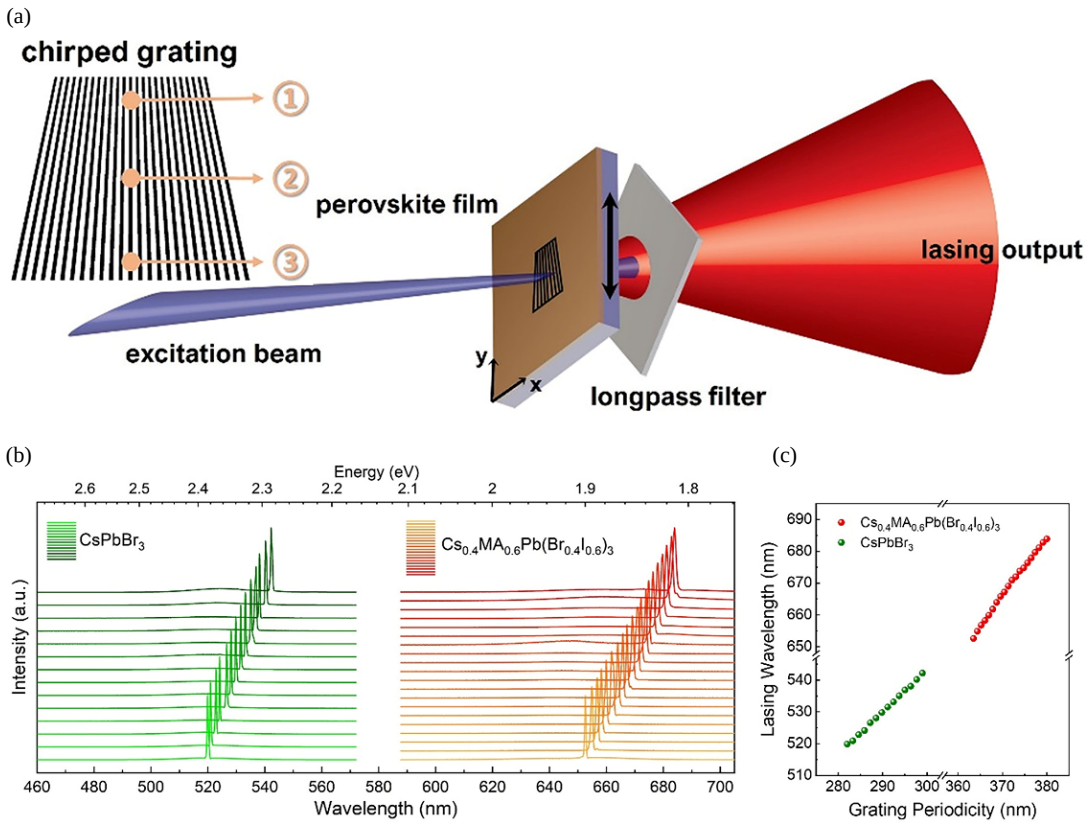

FIGURE 6. Description of the 1D chirped grating design, optical configuration, and lasing characteristics. (a) The schematic illustrates the chirped grating, with yellow circles marking the axis in increasing order including period variations at 350 nm, 440 nm, and 520 nm. The lower panel illustrates the optical pumping arrangement for surface-emitting perovskite DFB, where the perovskite film is adjusted along the y-axis with varying periods to capture tunable emission. (b) Displays recorded single-mode lasing from different positions of the chirped grating for $CsPbBr_3$ (green) and $Cs_{0.4}MA_{0.6}Pb\,(Br_{0.4}I_{0.6})_3$ (yellow-red) under a 355 nm pumping wavelength. (c) Illustrates the emission wavelength in correlation with grating periodicity [142].

range [16, 18]. In 2012, research on 2nd DFB gratings delved into dependencies on grating depth and gain medium, impacting laser wavelength and emission spectrum shape [138]. A comparative study on higher-order (2nd, 3rd, and 4th) polymer DFBs yielded insights by modifying grating depth and active film thickness, resulting in low-threshold lasing, variable slope efficiency, and diverse lasing patterns [59]. Aftenieva et al. recently utilized soft lithography to fabricate 2nd order DFBs based on CQDs and Langmuir-Blodgett arrangement, achieving a reduced lasing threshold of 0.6 mJ/cm^2 through optimization of geometric parameters [139].

Consequently, multi-wavelength operation in 1D DFB cavities is sought after in laser systems, and stacked DFB lasers employing different organic gain materials enable simultaneous operation in the blue and red spectrum [140]. Wavelength tuning is achieved by leveraging dependencies on grating period and layer thickness gradient, as demonstrated by a DFB laser attaining a 35 nm tuning range through a holographically produced grating with a deposited gain layer featuring a thickness gradient [141]. In 2018, Jung et al. designed a 1D CQDs DFB chirped grating, resulting in multi-wavelength lasing along the chirped direction with a lasing threshold of 400 μJ/cm^2 [126]. Roh et al. designed the practical and continuously adjustable single-mode lasing of a perovskite DFB microcavity laser across a wide spectral range at room temperature, relying on a substantial optical gain bandwidth ($\sim$ 90 meV) and a high modal gain coefficient (533 cm^{-1}), utilizing period-varying chirped Bragg gratings for precise tuning and achieving a low lasing threshold, (Fig. 6(a)) [142]. Figs. 6(b) and (c) show the optically pumped single mode lasing characteristics with continuous tunability from two different perovskites (green and red-yellow emission peaks), along with the tunable emissions range vs chirped grating periodicity (green and red circles, see Fig. 6(c). Beat structures with parallel gratings offer flexibility in adjusting laser patterns and the number of wavelengths, and in compound structures, ultralow thresholds can be achieved by balancing feedback and output coupling [127, 128]. In 2020, Zhai et al. fabricated a CQDs holographic dual-grating laser with first-order and second-order gratings, resulting in a lasing threshold nearly half that of conventional distributed feedback lasers [143].

3.1.2. 2D DFB Planar Feedback Cavity Lasers

Laser systems equipped with 2D DFB structures demonstrate considerable enhancements in feedback efficiency and lasing characteristics compared to their 1D DFB counterparts. The heightened interest in sophisticated diffractive resonators is

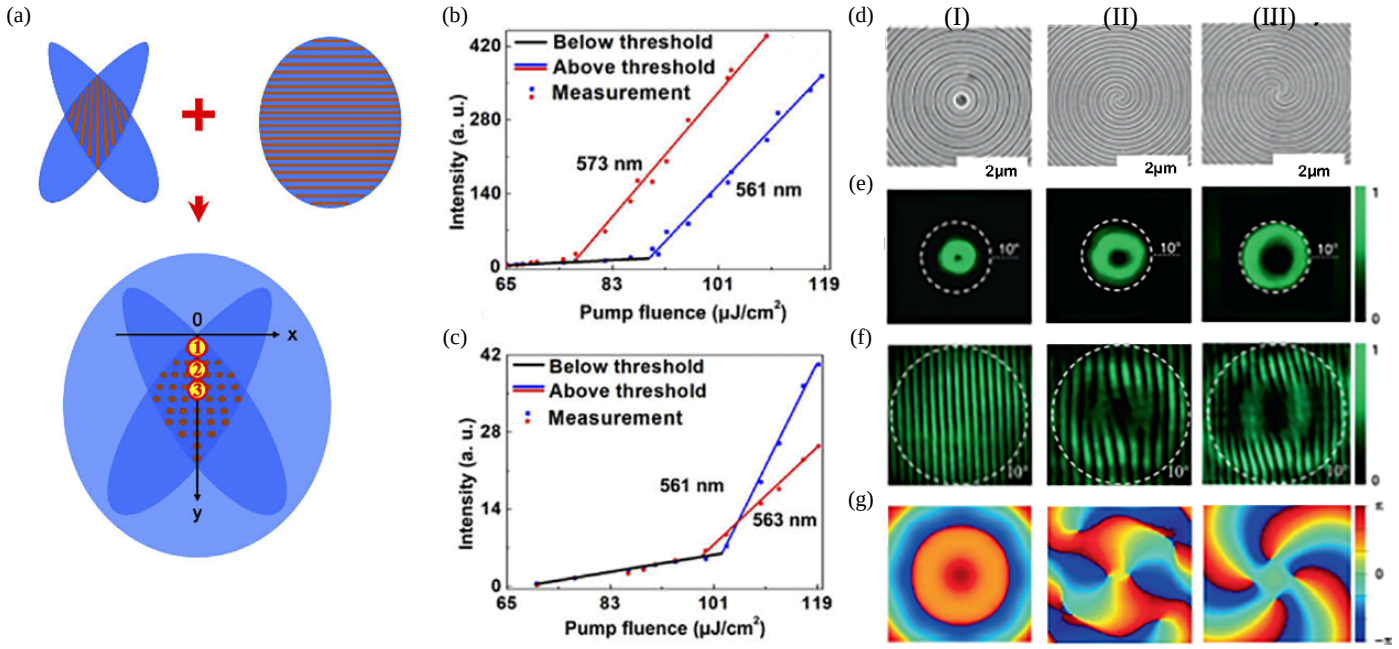

FIGURE 7. Examination of 2D compound chirped and perovskite vortex DFB lasers. (a) Illustration of 2D compound chirped cavities with periodic variation along the y-axis (marked by red circles from 1 to 3). (b), (c) Output intensity as a function of lasing threshold measured at different positions along the y-axis for the compound chirped cavity, (b) at $x = 0$ mm, $y = 2.7$ mm, and (c) at $x = 0$ mm, $y = 3.0$ mm. (d) Top-view SEM photograph of Archimedean spiral grating on VCSEL device displaying different topological charges: $I = 0$ (I), $I = 2$ (II), and $I = 4$ (III). (e), (f) Far-field intensity distributions and emission beams in the forward direction with self-interference profiles (measured at 21 μJ/cm^2). (g) COMSOL simulated phase distributions [154, 159].

rooted in their intricate designs, facilitating the application of 2D feedback within the active material film and allowing for feedback in various directions, owing to the inherent symmetry of the 2D pattern [144–148]. The 2D DFB microcavity technology achieves comprehensive 2D feedback by utilizing the 2nd order Bragg diffraction and concurrently serves as an output coupler through the 1st order Bragg diffraction. The main advantage of the 2D cavity is fine-tuning the laser's performance by adjusting cavity parameters, offering precise control over the intricate interplay between feedback and coupling. Compared to 1D feedback cavity, 2D DFB lasers demonstrate lower thresholds, higher wavelength numbers, and improved modes and patterns, alongside dynamic dispersion features that gracefully adapt to varying observation angles [17]. 2D DFB lasing can be achieved through different types of 2D photonic crystals, such as square, rectangular, triangular, honeycomb and hexagonal lattices, as well as fan-shaped, compound chirped, circular, and spiral gratings [124, 144, 149–154]. Multiple research groups utilized square lattices as DFB cavities, employing careful parameter design of grating period, mode analysis in k-space, and cavity coupling (the angle between two grating period) to manipulate radial/azimuthal polarizations and lasing threshold in the output beam [136, 155]. Zhai et al. developed a direct approach for rectangular DFB polymer lasers, achieving low-threshold emission by attaching a wet active layer to a DFB grating, and demonstrating both multiwavelength capability and versatility in polarization dependence within a 2D lattice cavity [150]. Other reports explore the use of a triangular lattice for achieving multiwavelength lasing in polymer DFB microcavity lasers, with the ability for continuous tuning through either mechanical adjustment to a soft substrate or by heating the lasing device [151, 156]. Guo et al. concentrated on laser operation within a honeycomb plasmonic lattice, pinpointing singlet and doublet mode, and showcased lasing at the K points by leveraging plasmonic lattice modes and two-dimensional feedback at high-symmetry points of the Brillouin zone [145]. Researchers have discovered that achieving continuous tunability across a broad spectrum is also possible by incorporating fan-shaped and chirped compound gratings. In 2020, Zhang et al. devised 1D and 2D chirped as well as compound chirped polymer DFB microcavities. They investigated the interactions among lasing modes and observed that 2D chirped cavities exhibited significantly broader wavelength tunability and increased lasing threshold with enhanced coupling strength, see Figs. 7(a)–(c) [154].

Circular grating DFB lasers achieve precise in-plane light control by employing omnidirectional feedback centered on the grating, establishing a frequency-specific photonic band gap. Recent research in this area has revealed compelling features, including single-mode lasing in thin films, minimal beam divergence ($\sim$ 10 mrad), and the emergence of a unique donut-shaped lasing pattern with azimuthal polarization [157, 158]. DFB lasers with spiral gratings offer precise wavefront manipulation, generating vortex beams with unique helical wavefronts and associated orbital angular momentum (OAM). In 2020, scientists incorporated Archimedean spiral gratings into per-

ovskite vertical-surface emitting laser (VCSELs), (Figs. 7(d)–(g)). This advancement allowed for the on-chip development of vortex microlasers with precisely controlled topological charges ranging from $q = 0$ to $q = 32$, marking a notable stride in perovskite VCSEL technology and enabling the precise manipulation of substantial OAM [159].

3.2. Bound States in Continuum (BICs) in Periodic Planar Feedback Cavities

The revolutionary notion of BICs has transformed our understanding of light-matter interactions and cavity design in photonics [160, 161]. BICs, characterized by exceptionally high-quality factors, defy conventional limitations by existing in open structures where radiation accessibility is permitted. The quest for an ideal cavity revolves around the concept of infinitely confining light at specific frequencies.

In the realm of photonics, the dynamics of BICs come into play when the frequency of a discrete optical mode stays outside the continuous spectrum of propagating waves. In such scenarios, light becomes entrapped within the cavity, unable to couple with the surrounding waves. Conversely, when the frequency of the discrete mode aligns with the continuous spectrum, the confined light couples with propagating waves, leading to leakage and diminished light confinement effectiveness. This concept of BICs traces back to 1929 when von Neumann and Wigner mathematically proposed the existence of a localized electronic state within the continuous radiation spectrum [162]. Over the ensuing century, this quantum mechanical concept has transcended its origins, finding applications in diverse fields, fostering the creation of electronic BICs, and holding promise for quantum mechanics and photonics [49, 163, 164].

BICs, which are dark optical states, have been successfully realized in various photonics systems such as gratings, waveguides, metasurfaces, and photonic crystals since their initial prediction in 2008 [165]. These optical BICs achieve an infinite quality factor (Q) by effectively isolating the state from external radiation channels, even as energy loss occurs in the resonator due to coupling with an external radiation channel. To support BICs, the systems must extend infinitely in at least one direction and possess a finite number of radiation channels [166]. The elimination of radiation coefficients can be accomplished through either symmetry mismatch or tuning independent parameters for destructive interference. The emergence of BICs is explained through concepts of symmetry mismatch or destructive interference. Symmetry-protected BICs, which remain confined as long as the system's symmetry is preserved, have been extensively explored in designs like metasurfaces and periodic assemblies including gratings and photonic crystals [167, 168]. Destructive interference, a fundamental mechanism for generating BICs, involves canceling two or more radiation channels in the far field. Fabry-Pérot BICs result from positioning resonators to form a cavity at a specific frequency or spacing, inducing destructive interference [169]. Friedrich-Wintgen (FW) BICs arise from the interference of resonances within the same resonator [170]. The inclusion of BICs in distinctive structures introduces optical feedback mechanisms, encompassing accidental BICs, merging BICs, and quasi-BICs within a singular resonator [49, 164]. Furthermore, BICs have been leveraged to enable novel lasing operations through their integration with optical gain materials. BIC-based lasers offer a distinct approach to manipulating laser characteristics, including directionality, beam shape, high-speed modulation, low threshold, and energy consumption.

3.2.1. Working Principle and Design for BICs Microcavity Lasers

Implementing optical BICs is a sensible approach to significantly minimize energy losses in the radiation channels of both 1D and 2D periodic microcavity lasers. Scientists have explored how BICs can improve the performance of 1D periodic planar feedback lasers with low thresholds, specifically utilizing CQDs as the gain medium, while preserving symmetry protection [171]. Their investigation centered on analyzing the electric field distribution of 2nd order DFB structures, revealing two distinct band edge modes, (Figs. 8(a) and (b)). These visual representations specifically emphasize TE-polarized waves and highlight the y-component of the electric field along the grating. Fig. 8(a) illustrates a mode with symmetry resembling a plane wave under normal incidence, allowing efficient coupling to the far field through diffraction. Conversely, the mode in Fig. 8(b) exhibits a different symmetry, impeding its coupling to the far field in the normal direction. The resultant asymmetry in Fig. 8(b) contributes to lower radiation loss, indicating a high Q factor. Theoretically, in an ideal system without absorption, scattering, or diffractive losses, the Q factor of this mode could reach infinity, classifying it as a symmetry-protected BIC. Additionally, by engineering the thickness of the CQD film, the grating-CQD slab can support both 1st-order and 2nd order waveguide modes (Fig. 8(c)), leading to a reduced lasing threshold and achieved a room-temperature lasing under 5-ns pulsed optical excitation [171].

Recently, Wang et al. conducted experiments to elucidate the operational principles behind the controlled fabrication of perovskite microlasers without the need for etching. This was achieved by applying a 1D polymer grating to a perovskite film, resulting in the formation of symmetry-protected BICs. The accompanying Fig. 8(d) explains a 1D BIC planar feedback cavity laser, comprising a substrate, perovskite waveguide, and 1D polymer grating. Key parameters, e.g., a waveguide thickness of 80 nm and grating dimensions (height, $H = 180$ nm, and period, $L = 290$ nm), were carefully chosen based on considerations of gain spectra and refractive index. Fig. 8(e) illustrates two resonance dips (546.5 and 510 nm, marked by red dash lines) in transmission spectra under oblique incidence. This study also performed simulations for both modes under oblique incidence and noted that the field patterns indicating waveguide modes traveling in opposite directions. With normal incidence, these modes gradually merge into a single dip (548.5 nm with a broader FWHM) [172]. The effective explanation of the interaction between these modes involves analyzing the coupling through a 2×2 matrix that considers two resonances [173]:

$$H = \begin{pmatrix} E_1 & W \\ V & E_2 \end{pmatrix} \tag{5}$$

$$E_{\pm} = (E_1 + E_2)/2 \pm \sqrt{(E_1 + E_2)^2/4 + VW},$$

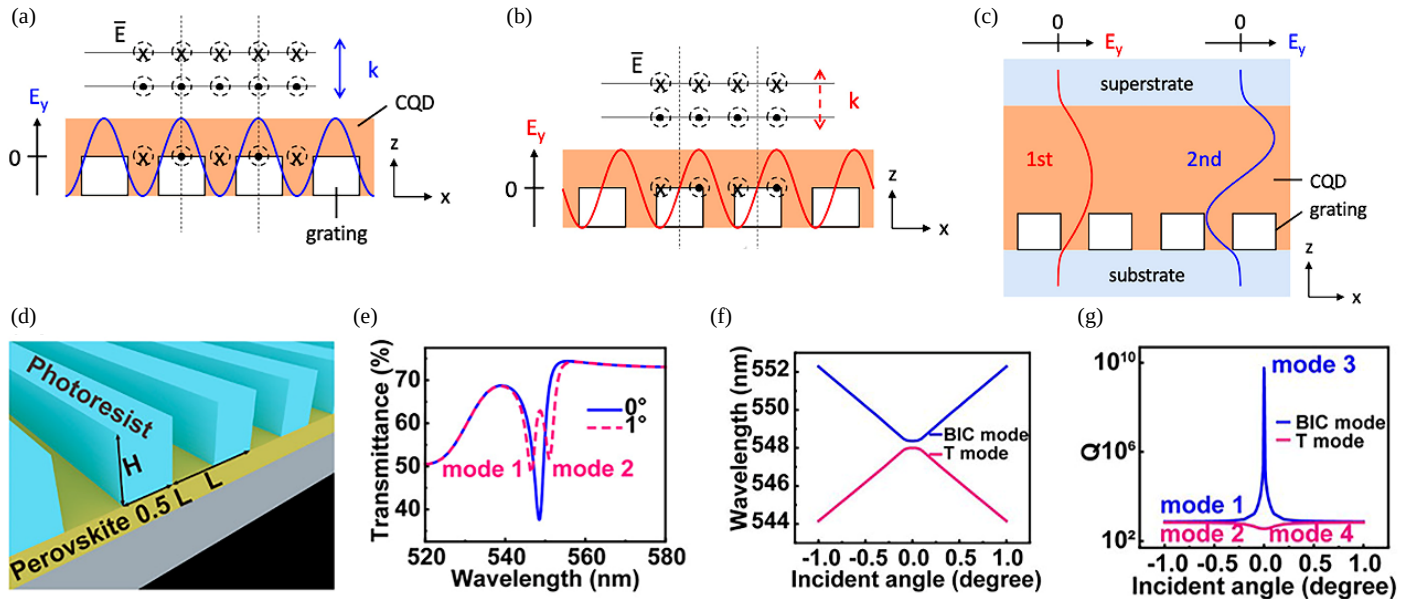

FIGURE 8. Demonstration of BICs in 1D CQDs and Perovskite cavity: Picture of TE-polarized second-order DFB modes — diffraction-coupled band-edge (a) and bound state in the continuum (BIC) (b). Illustrating Ey for standing waves along the x-axis, while $\bar{E}$ stands for standing wave as well as normal incident plane wave, highlighting the unique symmetry for BIC leading to minimal radiation loss. Solid and dashed arrows indicate k vector permissible and restricted radiation. (c) Conception of Ey for first- and second-order slab waveguide modes profiles in a grating coated with a thick film of CQDs. (d) Representation of etchless perovskites BICs device, featuring a grating duty cycle of 0.5. (e) Transmission graph at the normal (0°, single dip, blue solid line) and oblique (1°, two dips, red dash line). (f) Plots of wavelength vs incident angle for the two model configurations. (g) Graph of the Q factor as a function of a set of incident angles for two distinct modal configurations [171, 172].

$$(V \neq W^*) \tag{6}$$

$$E_{\pm} = E_1 \pm \sqrt{VW} \tag{7}$$

The energies E_1 and E_2 are two resonance energies, and V and W are coupling constants. When external coupling occurs, involving the interaction of two resonances with the external continuum, the coupling constant is typically represented as a complex quantity. As two resonances converge at their real components, a scenario emerges where E_1 equals E_2 in both the real and imaginary domains. Analyzing resonances at normal incidence, the study plotted eigenfrequencies against incident angles (Figs. 8(f) and (g)). Notably, at 0 degrees, two resonances repel, with one's Q factor decreasing and the other sharply rising to 10^9. Due to in-plane symmetry, the antisymmetric standing wave's radiation is suppressed in the far field. The high Q mode is attributed to a symmetry-protected BIC, mainly confined within the gain material — crucial for controlled etchless perovskite microlasers [172].

In PhCs planar feedback cavities, BICs fall into two main categories: symmetry-protected BICs and accidental BICs. Symmetry-protected BICs emerge under conditions of high symmetry, causing the separation of modes within different symmetry classes [174]. Conversely, accidental BICs may appear at non-zero wavevectors with additional symmetries, making their precise location challenging to predict, particularly in systems like square lattice photonic crystals [167]. In a 2013, Hsu et al. distinguished two specific BICs within a 2D Si_3N_4 photonic crystal slab. They observed a significant radiative Q factor at the Γ point and an exceptional Q factor of 1,000,000 for a confined BIC mode at around 35° [175]. In 2019, Jin et al. integrated symmetry-protected and accidental BICs in a high-Q Si photonic crystal cavity, introducing a novel BIC mode. Concentrating accidental BICs at the central Γ point and closely grouping all nine BICs amplified the Q factor, reducing scattering loss in momentum space and enhancing resilience against disturbances [176].

In 2021, Hwang and colleagues introduced a revolutionary laser design leveraging a super cavity mode formed by merging symmetry-protected and accidental BICs within the momentum space continuum. This approach enables the realization of an efficient laser with a small footprint based on a finite-size cavity, incorporating an infinite-size InGaAsP PhC slab with a square lattice array of air holes. The design features a TE-like band within the emission wavelength range of InGaAsP, and resonant modes converge in the lattice constant range of 560 to 590 nm. The radiation loss in this system follows specific laws (such as $[k(k-k_t)(k+k_t)]^2$, k^6, or k^2) depending on the lattice constant, influenced by the interaction of topological charges q_0 at the symmetry-protected BIC and q_t at the accidental BIC. The rapid sixth-order dependence of radiation losses on the wavevector is crucial for maintaining a high Q factor in a finite-size cavity hosting a BIC mode. The COMSOL simulations of the designed structure shown in Fig. 9(a) depict the magnetic field (Hz) mode profile at the Γ point of the fundamental TE-like band in a PhC slab with 15×15 periods. In contrast to the infinite-size cavity, the mode profile exhibits an envelope distribution with a convex shape, leading to mode leakage into free space and resulting in mode broadening

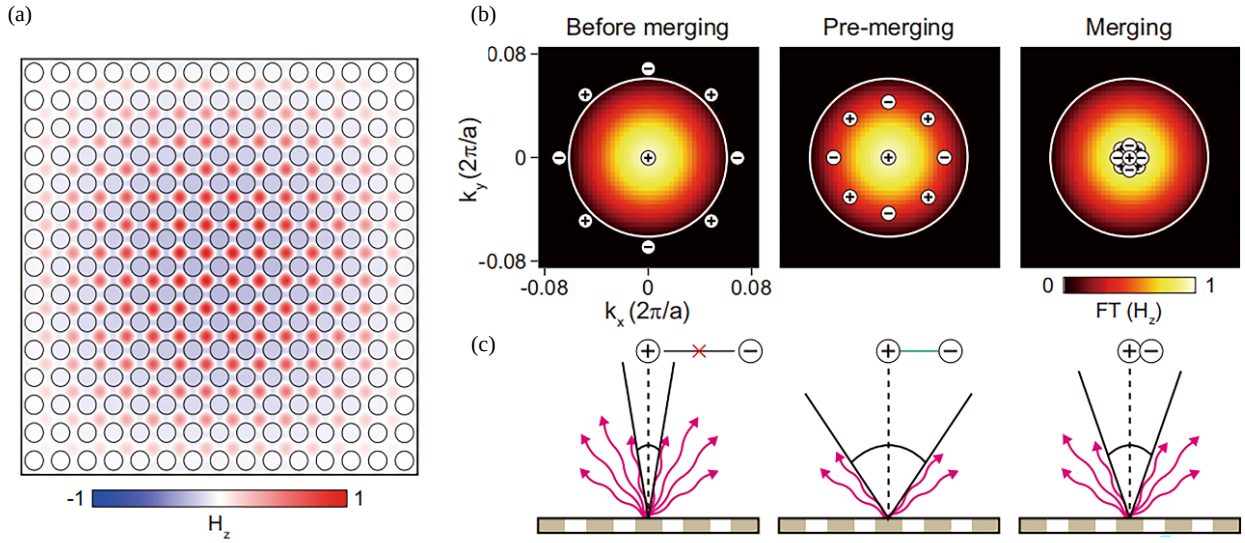

FIGURE 9. Concept of BIC in 2D periodic planar feedback cavity with finite dimensions: (a) COMSOL simulated Hz field with finite dimensions, e.g., $a = 573$ nm and $N = 15$ (represents period and number of air holes along the horizontal /vertical axis). (b) Topological charge variations in spatial Fourier transformation (FT) at different stages: before-merging (left), pre-merging (middle), and merging (right), with a 7° white circle demonstrating the first field minimum. (c) Schematic illustrations show the corresponding radiative loss scenarios aligned with the topological charge distributions in (b) [177].

Δk (white circle) in the k-space field distribution (FT(Hz) (see Fig. 9(b)). This finite-size effect leads to increased radiation loss due to mixing with off-Γ point modes with a finite Q factor. To enhance the Q factor, mitigating radiation loss caused by broadening (Fig. 9 (c)) is crucial. Undesired radiation loss at off-Γ points can be effectively suppressed by relocating the off-Γ BIC with charge q_t within the mode broadening range Δk (pre-merging regime) or to the Γ point $k = 0$ (merging regime). In the merging process with a limited number of air holes, the most effective radiation suppression is achieved by placing the charge q_t at an optimum k_t in the pre-merging configuration rather than at $k = 0$ (Fig. 9(c)) [177].

3.2.2. Recent Advances in BICs Periodic Microcavity Lasers

Harnessing BICs in lasers present revolutionary prospects, facilitating the development of microlasers with scalability, controllability, and directionality, marked by low thresholds and unique vector beam emissions arising from the inherent nonzero topological charges associated with BICs. The observed behaviors strongly reveal that surface-emitting lasers employ symmetry-protected BICs, featuring extensive coherent oscillations for precise control over the lasing pattern and achieving high-power emission. Wavelength-scale lasers, with low power consumption in high-Q BIC cavities minimizing radiative losses, offer potential for efficient active nanophotonic devices and incorporate unique cavity designs to control optical properties [49, 164].

Several groups are engineering intriguing features of BICs in 1D and 2D periodic microcavities and have realized multibeam, tunable emission wavelength, multiwavelength, and even directional lasing by optimizing cavity parameters [178–182]. In 2018, Ha et al. presented a directional BIC laser using gallium arsenide nanopillar arrays (100 nm diameter, 250 nm height), supporting vertical and in-plane dipole modes. They improved quasi-BIC Q factors by introducing higher diffraction orders in dielectric nanoantenna arrays, enabling controlled laser emission direction by tuning the nanoantenna array period along a primitive axis [178]. Wang et al. developed a 1D BICs etchless perovskite laser featuring a unique mode profile and high Q factor due to perovskite's exceptional gain. They fine-tuned parameters using COMSOL simulations and applied e-beam lithography to fabricate polymer gratings covering 80 nm $MAPbBr_3$ perovskite film, see Fig. 10(a). They observed the merging of two dips into single in transmission spectra during transition from oblique to normal incident, explained by the coupling between resonances. A comparative analysis of experimental and numerical outcomes is presented in a Fig. 10(c) displaying transmission spectra and the correlation between resonance angle and incident angle. Lasing characterization included far-field patterns and emission spectra analyzed with a frequency-doubled Ti: sapphire laser, see Figs. 10(b) and (d) [172]. Ha et al. reported a room temperature III–V semiconductor laser employing the BIC concept, achieving simultaneous multi-beam lasing with tunable wavelengths through guided-mode resonances and a grating structure [179]. In 2022, a study demonstrated off-Γ lasing utilizing the Friedrich-Wintgen (FW) BICs within a 1D suspended high-contrast grating. This laser exhibited an anti-crossing in the band diagram, allowing for low-threshold operation, angle-steering of laser beams, and tunable lasing directions through geometric modulation of FW-BIC conditions [180].

Scientists are actively exploring the utilization of 1D and 2D BIC planar feedback cavities to achieve single-mode lasing and decrease thresholds while realizing ultra-high Q fac-

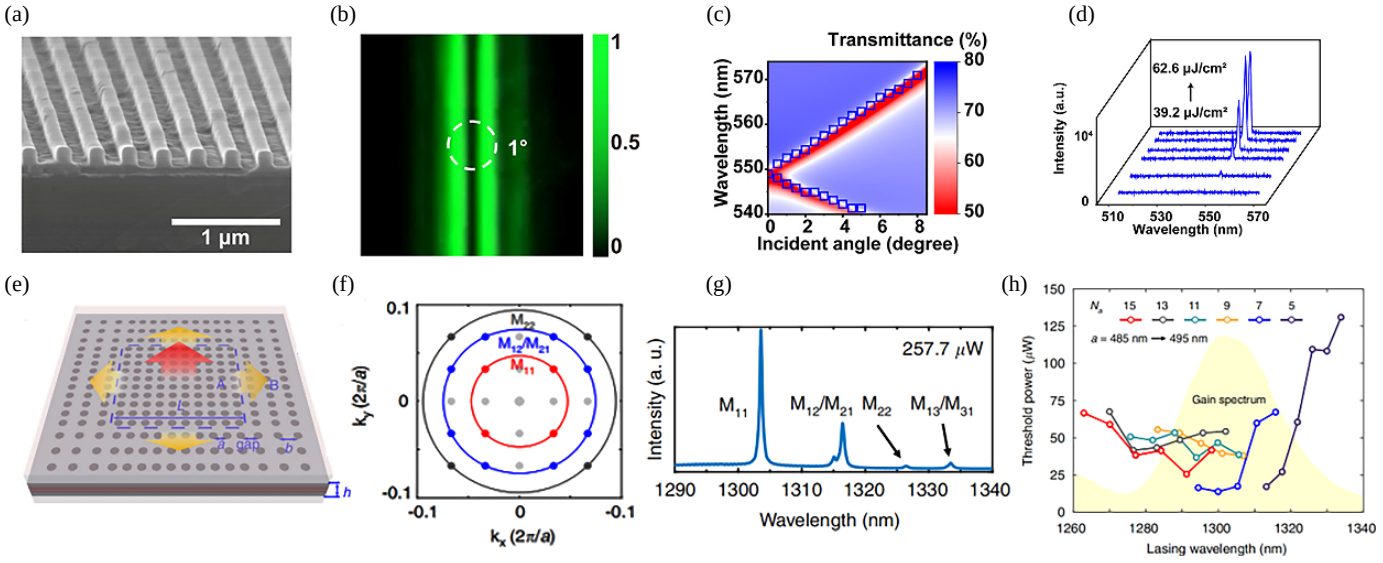

FIGURE 10. Experimental and theoretical analysis of lasing in 1D and 2D BICs microcavities: (a) Tilted SEM image of 1D etchless Perovskite BICs device. (b) Photograph of the experimentally measured angular distribution of the far field. (c) The relationship between incident angle (blue open circle) and wavelength, with numerical (red curve) calculations in the background. (d) Lasing spectra with increasing pump fluence. (e) A schematic diagram for photonic heterostructure exhibits two regions, e.g., mini-BIC cavity (A, $N_a \times N_a$, side length L, and period a) lies inside the bandgap region (B, width N_b, and period b), but both regions share the same periods ($a = b$). Here, the etched holes film gain medium is InAs/GaAs QDs with thickness ($h = 556$ nm). (f) Corresponding momentum arrangements of each mod as M_{pq} lie within the first quadrant of the momentum domain. (g) Recorded lasing spectra from the mini-BIC device ($a = 495$ nm and $N_a = 13$). (h) The relationship between the emission wavelengths and lasing threshold with varying cavity parameters. The shaded (yellow) area shows the QDs gain spectra [172, 186].

tors. They seek to identify new BIC modes, such as symmetry-protected, accidental, and super-BIC, by adjusting momentum space and cavity parameters [183–186]. In 2017, a groundbreaking development introduced room-temperature BIC lasers (1551 nm) employing a suspended semiconductor membrane with InGaAsP quantum wells. Lasing was maintained within a compact eight-by-eight cylindrical nano-resonator array, highlighting advantages like low threshold and room temperature functionality. Despite limitations in the array's size impacting momentum space modes and causing radiative loss, the challenge of downsizing remains relevant. For lasers and similar devices, a small finite footprint remains pivotal, emphasizing the necessity to maximize Q factors in realistic-sized cavities for optimal performance [183]. In 2021, researchers created a super-BICs cavity mode, merging symmetry-protected and accidental bound states in momentum space, resulting in an efficient laser with reduced threshold, higher Q factor, and smaller far-field images. This advancement tracked the evolution of lasing properties through lattice spacing variations [177]. In a recent achievement, researchers demonstrated room-temperature continuous-wave BIC lasers at 1310 nm in the O-band. This was accomplished by utilizing a miniaturized BIC cavity within an InAs/GaAs epitaxial QDs gain membrane, effectively trapping light in the transverse direction, as depicted in Fig. 10(e). This design, preventing lateral leakage, achieved an ultra-low threshold of 12 μW at room temperature, enabling single-mode lasing in compact cavities with a mode volume of $1.16(\lambda/n)^3$. The accompanying Figs. 10(f)–(h) illustrate momentum space distribution, emission wavelength of various modes (at pump fluence of 257.7 μW), and lasing threshold vs tunable wavelength at different cavity parameters [186].

Further research investigating optical vortex beams, carrying quantized OAM offers significant potential in diverse applications. The challenges observed in vortex microlasers, such as reduced Q factors with spiral waveguides or micro-pillar chains and added scatterers, have been addressed by Bahari et al. They demonstrated controllable vortex lasers with distinct far-field patterns by leveraging BICs, creating a steerable-by-design system through manipulation of topological charges and continuous BIC movement via hole radius tunings [187]. Recent findings highlight the ability of topologically protected charges in BIC modes to enable low-energy consumption and high-speed optical modulations in vortex beams. Huang et al. introduced perovskite-based vortex microlasers with a BIC structure, reaching high Q factors and low lasing thresholds. This design allowed for room temperature all-optical switching and controlled emission profiles by varying pump laser arrangements [188]. Investigators utilized substantial field enhancement at the Γ point, along with the chirality of the C points, to create an efficient approach for chiral emission. This resulted in the realization of chiral PL and lasing, which exhibits notable features like high handedness purity, directionality, and Q factor [189]. In 2022, Tian et al. designed subwavelength-thin phase-change perovskite BIC metasurface laser. This versatile and tunable micro-laser studied the generation of reversible polarization vortexes, attributed to substantial fluctuations in refractive index and gain during structural phase transformations in the perovskite material, (Fig. 11) [190]. Tang et al. developed

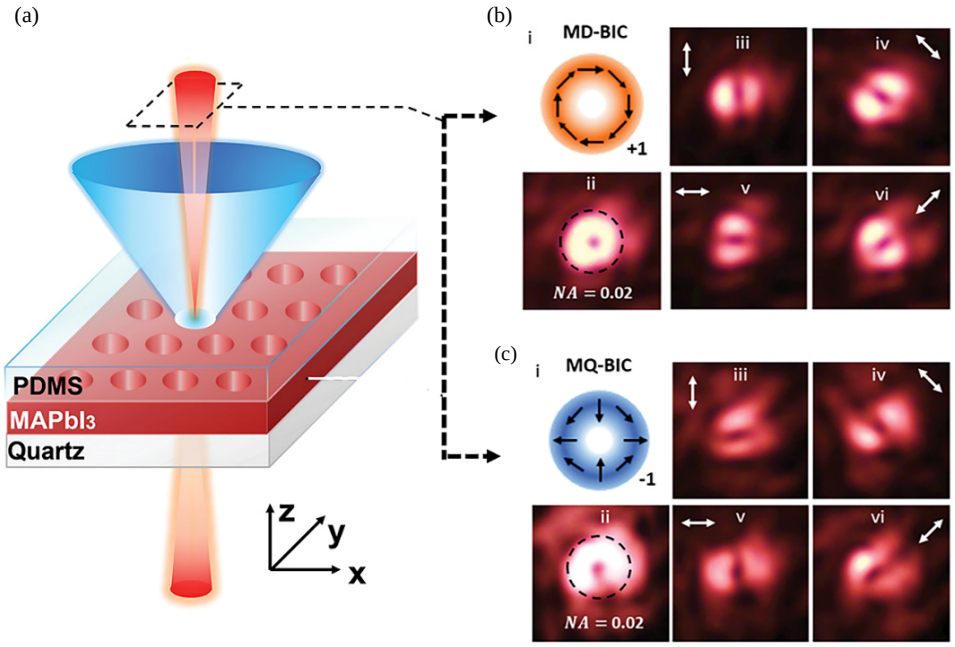

FIGURE 11. Micro-laser employing phase-change perovskite with a variable topological polarization singularity: (a) Schematic representation of a micro-laser with tunability, relying on a BIC metasurface incorporating phase-change perovskite. (b) Visualization for $+1$ topological charge TE polarized light (i); room temperature far-field profile (donut-like patterns) without a polarizer (ii); Recorded far-field profiles using polarizer at different angles (iii)–(vi). (c) Visualization for $+1$ topological charge TM polarized light (i); 135 K far-field profile without a polarizer (ii); recorded far-field profiles using polarizer at different angles (iii)–(vi) [190].

a revolutionary technique by combining BICs with photonic bandgaps, resulting in a low-threshold quasi-BICs single-mode PhC laser. Constructed on a hybrid platform of CQDs and SiO_2, the laser efficiently assembles emission within ± 1.85 degrees of the normal surface direction [191].

3.3. Quasiperiodic Microcavity Lasers

Optical deviations from periodicity, as observed in photonic quasiperiodic structure, yield unexpected outcomes marked by sharp diffraction patterns, even in the absence of translational symmetry [116, 192, 193]. Recent studies have exposed a new class of materials known as "deterministic aperiodic" structures, coexisting alongside both crystalline and amorphous counterparts. These assemblies, formed through a substitution rule involving two fundamental components, display long-range order without translational symmetry. They can be subdivided into quasiperiodic (group A) and other deterministic aperiodic geometries (group B). QPs geometries (nD, where $n = 1$, 2, or 3) are precisely defined by their generation through substitution and formation via partial projection from a higher dimensional space (mD, where $m > n$). In the 1D context, quasiperiodic geometries in group A, like the Fibonacci Octonacci sequence, reveal specific repeating patterns. In contrast, group B comprises aperiodic structures for example the Thue-Morse and Rudin-Shapiro sequences, lacking regular repetition [194, 195]. Both groups display discrete Fourier components, while group B structures exhibiting more intricate Fourier properties. The groundbreaking discovery of quasicrystals by Shechtman et al. in 1984, complemented by the theoretical model from Levine and Steinhardt, established the foundation for the field [196, 197]. Kohmoto et al. made a significant involvement by unveiling the first optical aperiodic system — a 1D QPs displaying long-range order, fabricated using dielectric multilayers to form the Fibonacci sequence [198]. The structure factor F(k) for an object is derived by applying a Fourier transform to its spatial configuration in real space, involving the summation over the positions of 'atomic' elements denoted as R_n:

$$F(k) = \lim_{N\to\infty} N^{-1} \sum_{R_n} \exp(ik \cdot R_n) \tag{8}$$

Consequently, confirming the existence of long-range order in a structure implies that its $F(k)$ contains specific Fourier components, commonly known as reciprocal vectors (RVs). In reciprocal space, both periodic and quasiperiodic structures exhibit distinct RVs, with changes in the geometric arrangement in real space influencing these variations [199]. In the literature, the investigation of 1D quasicrystals within dielectric media involved employing multilayer stacks with two different permittivity (ε_1 and ε_2) arranged in Fibonacci and Octonacci sequences, identified as non-resonant and resonant cases, exhibit's phenomena such as photoluminescence and lasing. Higher dimensional photonic quasicrystals, characterized by long-range deterministic assemblies and rotational symmetry exceeding 14-fold, demonstrate enhanced flexibility in geometric design compared to their 1D quasi-periodic counterparts [50, 200, 201]. This unique characteristic positions them

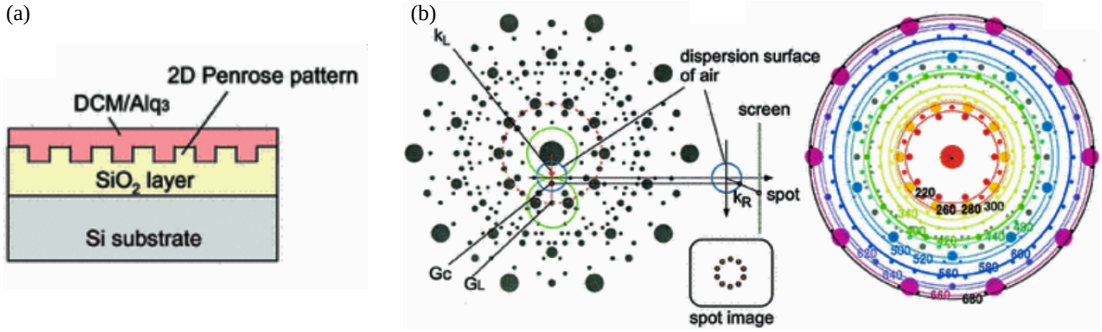

FIGURE 12. Design and operating principles of 2D QPs lasers: (a) Schematic of 2D Penrose microcavity laser. (b) Visualization of lasing characteristics of QPs based on the reciprocal lattice condition. Diffraction coupling with G_c induces out-of-plane emission in the k_R direction under lasing conditions with G_L (left side panel). Numerous colors signify spot images for reciprocal lattice points and $2k$ circles (Right side panel) [209].

as highly promising for diverse applications in optoelectronics and micro-nanoscale cavity lasing devices.

3.3.1. Principal and Design of QPs Planar Feedback Cavities

Quasiperiodic assemblies, arising from a deterministic rule, blend non-periodic behaviors with optical features bridging disordered and periodic assemblies [50]. Specifically, Fibonacci-type QPs assemblies exhibit a Cantor set energy band with zero Lebesgue measure, implying singular continuity in large samples [202] Researchers have designed 1D Fibonacci QP assemblies by stacking dielectric materials with distinct permittivity (ε_A and ε_B) and thicknesses (L_A and L_B), considering non-resonant and resonant cases [203, 204]. Investigations into transmission, reflection, and photoluminescence spectra reveal intriguing features when the incident frequency aligns with resonances, including 2D exciton frequencies and the quasi-periodic pseudo-gap [204]. In the generation of 1D Fibonacci QPs, segments A and B, distinguished by lengths L_A (longer) and L_B (shorter), undergo iterative rules $A \to B$ and $B \to BA$, resulting in an ordered, infinite sequence. This process follows a recursion relation: $S_{j+1} = (S_{j-1}S_j)$, with $j > 1$ for $S_0 = \{A\}$ and $S_1 = \{B\}$. Fibonacci's structure factor, featuring discrete Fourier components (RVs), contributes to sharp diffraction Bragg peaks, densely filling k space. In an infinite Fibonacci set, these components are located at $Q_{hh'}$, determined by two independent integers (h and h'):

$$Q_{hh'} = 2\pi d(m + n/\tau) \tag{9}$$

where $d = L_B(3-\tau^2)$ is the mean period, and $\tau = L_B/L_A$ represents the golden ratio. Researchers have precisely calculated the Fourier component ($f_{hh'}$) of the Fibonacci sequence related to $Q_{hh'}$ [50, 205]. In the non-resonance case, the dielectric constant $\varepsilon(z)$ is expressed by Fourier components ε_G, represented as $\varepsilon(z) = \sum_G \varepsilon_G \exp iG \cdot z)$ where $G = \pm Q_{hh'}$, with ε_G acting as the structure factor [206]. Poddubny et al. introduced a theoretical model of resonant 1D photonic Fibonacci QPs using a multi-quantum well setup, uncovering 'super-radiance' behavior and unique optical modulation features not present in periodic counterparts [207]. Subsequent experimental validation with GaAs quantum well (QW) stacks in canonical and non-canonical Fibonacci sequences showcased advantages, emphasizing robust emission within the pseudo-gap and distinct spectral features compared to periodic structures [204].

The research in quasiperiodic assemblies enables scientists to further investigate their lasing behavior encompassing 1D, 2D, and even 3D assembles. Mahler et al. pioneered the first QPs DFB laser, integrating a Fibonacci sequence into a 1D grating that operates in the terahertz range with electrical pumping. This integration involves replacing material interfaces with Fibonacci type slits in the top metal with equal periods, acting as essential scatterers that alter the waveguide to align with inter-sub-band transition selection laws. The lasing mechanism was explained based on the reciprocal lattice vector ($k = F(i)/2$) at the band edges. Eigenfrequencies analysis for the 12th order Fibonacci sequence revealed a weak dependency of the optical bandgap on slit width, distinguishing it from similar periodic gratings. The study also reveals the scaling of the laser wavelength with the Fibonacci dimension. Broadening the gain spectrum led to multi-wavelength lasing, attributed to the increased number of wave vectors linked with diverse RVs (or $F(i)$) in the Fibonacci sequence, better matching the prolonged gain spectrum [209]. Notomi et al. engineered 2D PhC QP lasers featuring Penrose patterns, exhibiting coherent lasing and diverse 10-fold-symmetric spot patterns without translational symmetry. They accomplished this by designing a Penrose-type hole pattern on a SiO_2 substrate and covered with a thin film of DCM-doped Alq_3 (Fig. 12(a)). The lasing mechanism was explained through the discrete RVs. This is similar to the standing wave phenomenon within the RVs space: $\sum(k - G_j) = 0$. For instance, when the diffraction spots in QPs share the same origin, they can be evaluated from the lasing frequency (ω_L) and RVs points. By considering a single lasing mode (G_L), that makes a dispersion circle in the air having a radius $\omega a/ck_o$ centered at G_L. If the major RVs G_c point is present in the same circle, then the corresponding lasing mode can be radiated parallel to k_R on the dispersion sphere [$k_R = (G_L - G_c)$], see left panel of Fig. 12(b). Reciprocal lattice colors categorize symmetry patterns of spot images, indicating that the diverse types are influenced by the local configuration around lasing mode G_L due to the non-identical nature of most reciprocal lattice points in QPs, see right panel of Fig. 12(b) [208]. In 2021, Hayat et al. introduced a pentagonal prism designed for interference holography, aiming to enable

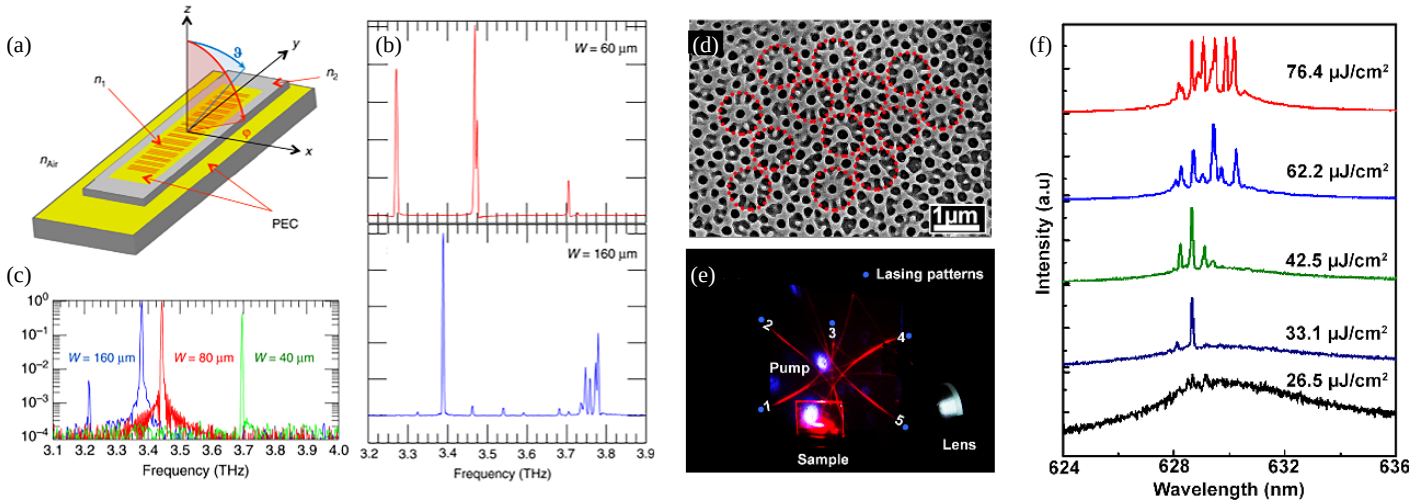

FIGURE 13. Experimentally observed lasing properties from 1D and 2D QPs microcavity lasers: (a) Schematic shows a 3D view of the device patterning 1D Octonacci sequence (red lines) on the top. Recorded emission peaks at varied electrically pumped fluences; (b) multi-wavelength emissions, (c) single wavelength emissions. (d) SEM of 2D QPs microcavity illustrating 10-fold rotational symmetry. (e) Experimentally recorded photograph of multi-wavelength lasing patterns upon optically pumping. (f) The emergence of multi-wavelength due to increasing pump fluence [210, 223].

multi-wavelength lasing within a 2D CQD QPs microcavity while maintaining 10-fold rotational symmetry. The analytical model proposed involves distributing five independent grating structures symmetrically in the 2D space, each functioning as a single DFB laser. Additionally, the model accounts for the cavity coupling effect between adjacent cavities and predicts about the multiwavelength-wavelength emissions [210].

Further, the functionality of lasers in PhC QP assemblies has been successfully demonstrated by generating localized modes known as single-cell cavity modes. This approach selectively populates a few holes in the 2D QCs hole array with an optical gain medium, confining laser modes. This laser process is analogous to a defect mode, where lasing specifically occurs within the optical gap [211, 212]. In 2021, Cui et al. introduced a 1D Fibonacci-spaced defect microcavity, incorporating cavity coupling in their study. Their analytical model predicts essential parameters in microcavity lasers — such as mode number, eigenfrequency, and Q factor. Aligned with FDTD simulations, the results reveal a substantial increase in the Q factor with the emergence of confined optical modes [213].

3.3.2. Recent Advance in QPs Microcavity Lasers

Recent research has explored lasing behavior in diverse QPs microcavities, incorporating complex geometries such as 2D Penrose tiling, 1D Fibonacci and Octonacci sequences, defect points, long-range rotational symmetries, and 3D icosahedral structures [208, 209, 214–222]. These intricate designs have led to significant advancements in lasing performance, characterized by lower thresholds, efficient feedback in various directions, robust localization of optical modes, emission independence at different surface angles, and minimized beam divergence, resulting in distinctive and well-defined lasing patterns.

In the past twenty years, researchers have made notable advancements in exploring lasing characteristics within various planar feedback cavities employing QP structures. Particularly, within the wavelength range of 500–600 nm, researchers have successfully achieved lasing with diverse patterns within the 2D Penrose lattice. This achievement was made possible by manipulating the lattice constant (a, ranging from 180 to 660 nm) for DCM-doped Alq_3 as the gain medium [209]. The performance of electrically pumped terahertz quantum-cascade lasers has seen significant enhancement through the utilization of Penrose-tiled 2D photonic quasicrystals. This improvement has resulted in peak powers of 65 mW and 0.1–0.2% wall-plug efficiencies. Consequently, this advancement has facilitated the generation of unique conical beam profiles originating from the intricate quasicrystal Fourier spectrum [223].

In 2020, scientists optimized lasing properties in an electrically pumped 1D surface-emitting quantum cascade terahertz laser, utilizing a top metal grating arranged in an 8^{th} order Octonacci sequence to provide necessary feedback (Fig. 13(a)), boosting output power (240 mW), and achieving a wall-plug efficiency ($\eta \approx 1\%$). Controlled surface emitting lasing, switching between single and multi-mode over a broad frequency range (bandwidth of 530 GHz), was achieved by varying ridge width and related aperture length (Figs. 13(b) and (c)) [223]. Achievements in lasing have been reported in microcavities characterized by octagonal, 12-fold, and 8-fold quasiperiodic structures, attributed to the incorporation of single defects like central air holes or omitting 7^{th} or 9^{th} holes within the cavity. These modifications support whispering gallery modes, resulting in notable characteristics such as low thresholds, high Q factors, and the ability to exhibit both single-mode and multi-mode lasing [211, 218, 224].

Researchers have employed multi-beam or holographic lithography to design various quasiperiodic (QPs) microcavities with long-rotational symmetries, demonstrating compelling lasing behaviors such as low thresholds, multi-wavelength emission, and visually appealing patterns with minimal beam divergence [219, 221, 225–228]. In 2021,

Hayat et al. used holographic lithography to achieve a 10-fold rotational symmetric QPs laser using a specially designed pentagonal prism coated with colloidal quantum dots (CQDs) nanomaterials (Fig. 13(d)). The resulting microcavity exhibited multi-wavelength emission when optically pumped by a 343 nm short-pulse laser (1 ns and 800 Hz), featuring a linear increase in pump fluence and revealing five lasing patterns with a star-like shape in the middle (Figs. 13(e) and (f)) [210].

Furthermore, a seven-beam interference holography method was employed to fabricate 3D dye-doped icosahedral quasicrystals (QPs) lasers using dichromate gelatin suspension. These samples displayed well-defined multi-directional lasing spots with distinctive icosahedral symmetry upon optical pumping [63].

4. FUTURE DEVELOPMENTS

Research on periodic and quasiperiodic planar feedback micro-nanoscale lasers has progressed significantly over decades, leveraging diverse micro-nanoscale cavities and lasing materials. However, attention is warranted to address challenges hindering the commercialization of such devices.

There's a need to concentrate on high-performance micro-nanoscale cavities. The current output power is constrained by the small pumping volume and large cavity size. To overcome this, diverse periodic and quasiperiodic architectures should be explored to enhance light-matter interaction, minimize losses, and improve light coupling for higher output efficiencies and continuous wave lasing. Essential features like frequency repetition rate, material stability, reliability, and lifetime require further exploration.

Ongoing research focuses on dynamic developments in DFB, BICs, and QPs planar feedback cavities, expanding their applications to sensing, imaging, optical networks, and amplifiers [229–234]. DFB lasers, for instance, find utility in gas sensing and biomedical diagnostics due to their tunable, stable, and narrow linewidth emissions [235–237]. More recently, Sano et al. integrated multiple on-chip DFB lasers with fluorescence biomarker detection, removing the need for fiber alignment systems and allowing for complex multiplexed sensing experiments [238]. In 2018, Buckley et al. designed a high-power DFB laser for Terabit optical interconnect which include eight channel wavelength-division-multiplexed. The device operated at 1280 nm wavelength which achieved record high power laser emissions (> 250 mW) and efficiency about 36% [239]. BIC microcavity lasers, utilizing non-radiative states, enhance sensitivity in applications like refractive index sensing, making them well-suited for biosensing and label-free biomolecule detection [240, 241]. Zhang et al. introduce a 2D micro-laser with high gas detection sensitivity through BIC, featuring a wavelength shift tied to refractive index changes and a remarkable figure of merit at 4420 RIU^{-1} [242]. Further research has successfully employed a technique maintaining quasiperiodic structured illumination in microscopy for precise recovery of mouse brain neuron structures in challenging conditions, including deep tissue imaging with low SNR and sparse samples [243]. However, current applications rely on optical pumping, posing integration challenges with lab-on-chip platforms. Future efforts should focus on engineering strategies to facilitate practical applications and integration into lab-on-chip platforms.

Electrical pumping remains challenging due to intrinsic properties of luminescent materials and loss channels within micro-nanoscale cavities. Future developments should address these challenges to enable efficient electrical pumping and broaden the scope of applications for these devices.

5. CONCLUSION

This review examines a range of microcavity designs and operational principles applicable to both periodic and quasiperiodic subwavelength structures. The focus is on customizing laser performance, encompassing aspects such as lasing threshold, patterns, mode selection, directional lasing, and vortex beam lasing. These microcavities exhibit high-quality factors and small mode volumes, effectively combined with luminescent materials like organic and inorganic compounds, laser dyes, quantum dots, and perovskites, enabling the development of efficient lasers across a broad spectrum from ultraviolet to telecommunication wavelengths. Over the past few decades, diverse configurations of distributed feedback (DFB) lasers utilizing periodic gratings as feedback channels have significantly influenced overall lasing behavior. These configurations, spanning 1D, 2D, and 3D DFB microcavities, not only reduce lasing thresholds but also enable tunable emissions, diverse lasing patterns, spatial mode distribution, multiwavelength lasing, low beam divergence, and the generation of vortex beams with helical wavefronts. An avenue of exploration involves periodic microcavities capable of achieving BICs lasers with infinitely high Q factors. This is achieved by eliminating non-radiative states from external channels despite energy loss from external radiation channel coupling. Different types of BICs — such as symmetry-protected, accidental, quasi, and super — can be obtained by engineering cavity parameters, introducing novel lasing characteristics such as ultra-low thresholds, directional lasing, and vortex beam lasing. Additionally, quasiperiodic microcavities, positioned between periodic and random structures, demonstrate sharp diffraction patterns. Their lasing behavior can be elucidated through reciprocal lattice considerations. Exploration of diverse configurations in quasiperiodic microcavities reveals long-range rotational symmetries, leading to optimal lasing features such as low lasing thresholds and intricate lasing patterns. This comprehensive analysis underscores the rich potential of both periodic and quasiperiodic microcavities in tailoring laser performance across various parameters and spectral ranges.

ACKNOWLEDGEMENT

The work is partially supported by the National Key Research and Development Program of China (No. 2022YFC3601002), the "Pioneer" and "Leading Goose" R&D Program of Zhejiang (Nos. 2022C03051, 2023C03083, 2023C03135), and the Zhejiang Provincial Natural Science Foundation of China (No. LDT23F05014F05). The authors are grateful to Dr Julian Evans of Zhejiang University for helpful discussions.

REFERENCES

[1] Kim, T.-I., J. G. McCall, Y. H. Jung, X. Huang, *et al.*, "Injectable, cellular-scale optoelectronics with applications for wireless optogenetics," *Science*, Vol. 340, No. 6129, 211–216, 2013.

[2] Miller, D. A., "Device requirements for optical interconnects to silicon chips," *Proceedings of the IEEE*, Vol. 97, No. 7, 1166–1185, 2009.

[3] Smit, M., J. Van der Tol, and M. Hill, "Moore's law in photonics," *Wiley Online Library*, 1–13, 2012.

[4] Hagley, E. W., L. Deng, M. Kozuma, J. Wen, K. Helmerson, S. L. Rolston, and W. D. Phillips, "A well-collimated quasi-continuous atom laser," *Science*, Vol. 283, No. 5408, 1706–1709, 1999.

[5] Aveline, D. C., J. R. Williams, E. R. Elliott, C. Dutenhoffer, J. R. Kellogg, J. M. Kohel, N. E. Lay, K. Oudrhiri, R. F. Shotwell, N. Yu, and R. J. Thompson, "Observation of Bose-Einstein condensates in an Earth-orbiting research lab," *Nature*, Vol. 582, No. 7811, 193–197, 2020.

[6] Gu, Y., C. He, F. Liu, and J. Ye, "Raman ink for steganography," *Advanced Optical Materials*, Vol. 9, No. 6, 2002038, 2021.

[7] Doble, P. A., R. G. d. Vega, D. P. Bishop, D. J. Hare, and D. Clases, "Laser ablation — Inductively coupled plasma — Mass spectrometry imaging in biology," *Chemical Reviews*, Vol. 121, No. 19, 11 769–11 822, 2021.

[8] Letokhov, V. S., "Laser biology and medicine," *Nature*, Vol. 316, No. 6026, 325–330, 1985.

[9] Ouyang, J., P. T. Mativenga, Z. Liu, and L. Li, "Energy consumption and process characteristics of picosecond laser decoating of cutting tools," *Journal of Cleaner Production*, Vol. 290, 125815, 2021.

[10] Fleet, L., "Dreaming of death rays: The search for laser weapons," *Nature*, Vol. 565, No. 7738, 158–160, 2019.

[11] Wang, T., C. Jiang, Q. Fang, X. Guo, Y. Zhang, C. Jin, and S. Xiang, "Reservoir computing and task performing through using high-β lasers with delayed optical feedback," *Progress In Electromagnetics Research*, Vol. 178, 1–12, 2023.

[12] Maiman, T. H., "Stimulated optical radiation in ruby," *Nature*, Vol. 187, 493–494, 1960.

[13] Soffer, B. H. and B. B. McFarland, "Continuously tunable, narrow-band organic dye lasers," *Applied Physics Letters*, Vol. 10, No. 10, 266–267, 1967.

[14] Karl, N., "Laser emission from an organic molecular crystal," *Physica Status Solidi A*, Vol. 13, No. 2, 651–655, 1972.

[15] Avanesjan, O. S., V. A. Benderskii, V. K. Brikenstein, V. L. Broude, L. I. Korshunov, A. G. Lavrushko, and I. I. Tartakovskii, "Anthracene crystals under intensive optical pumping," *Molecular Crystals and Liquid Crystals*, Vol. 29, No. 1, 165–174, 1974.

[16] Samuel, I. D. W. and G. A. Turnbull, "Organic semiconductor lasers," *Chemical Reviews*, Vol. 107, No. 4, 1272–1295, 2007.

[17] Fu, Y. and T. Zhai, "Distributed feedback organic lasing in photonic crystals," *Frontiers of Optoelectronics*, Vol. 13, 18–34, 2020.

[18] Kuehne, A. J. C. and M. C. Gather, "Organic lasers: Recent developments on materials, device geometries, and fabrication techniques," *Chemical Reviews*, Vol. 116, No. 21, 12 823–12 864, 2016.

[19] Liang, N., J. Yan, and T. Zhai, "Hybrid microcavity lasers: Principle, design, and practical application," *Laser & Photonics Reviews*, Vol. 17, No. 11, 2300343, 2023.

[20] Park, Y.-S., J. Roh, B. T. Diroll, R. D. Schaller, and V. I. Klimov, "Colloidal quantum dot lasers," *Nature Reviews Materials*, Vol. 6, No. 5, 382–401, 2021.

[21] Wang, D. and A. Yang, "Emerging optics from structured nanoscale optical cavities," *arXiv preprint arXiv:2307.12587*, 2023.

[22] Zhang, H., W. Zhao, Y. Liu, J. Chen, X. Wang, and C. Lu, "Photonic-plasmonic hybrid microcavities: Physics and applications," *Chinese Physics B*, Vol. 30, No. 11, 117801, 2021.

[23] Bravo-Abad, J., A. Rodriguez, P. Bermel, S. G. Johnson, J. D. Joannopoulos, and M. Soljačić, "Enhanced nonlinear optics in photonic-crystal microcavities," *Optics Express*, Vol. 15, No. 24, 16 161–16 176, 2007.

[24] Wang, Z., R. Yu, C. Pan, Z. Li, J. Yang, F. Yi, and Z. L. Wang, "Light-induced pyroelectric effect as an effective approach for ultrafast ultraviolet nanosensing," *Nature Communications*, Vol. 6, No. 1, 8401, 2015.

[25] Zhang, Y., M. Hu, and Z. Wang, "Enhanced performances of p-si/n-ZnO self-powered photodetector by interface state modification and pyro-phototronic effect," *Nano Energy*, Vol. 71, 104630, 2020.

[26] Li, Y.-Z., Z. Zhang, H. Chen, and F. Gao, "Polarization-wavelength locked plasmonic topological states," *Polarization*, Vol. 2023, 9–25, 2023.

[27] Lee, Y.-H., J. L. Jewell, A. Scherer, S. L. McCall, J. P. Harbison, and L. T. Florez, "Room-temperature continuous-wave vertical-cavity single-quantum-well microlaser diodes," *Electronics Letters*, Vol. 25, No. 20, 1377–1378, 1989.

[28] Jukam, N., "A wavelength-size tunable Fabry-Pérot laser," *Nature Photonics*, Vol. 13, No. 12, 823–825, 2019.

[29] Ra, Y.-H., R. T. Rashid, X. Liu, S. M. Sadaf, K. Mashooq, and Z. Mi, "An electrically pumped surface-emitting semiconductor green laser," *Science Advances*, Vol. 6, No. 1, eaav7523, 2020.

[30] Man, J., N. Zhu, H. Zhang, K. Sun, J. Ke, W. Han, W. Chen, Y. Liu, X. Wang, H. Yuan, and L. Xie, "An electrical-filtered optical heterodyne technique for tuning speed measurement of DBR lasers," *Chinese Science Bulletin*, Vol. 56, 704–708, 2011.

[31] Xu, Z., T. Zhai, X. Shi, J. Tong, X. Wang, and J. Deng, "Multifunctional sensing based on an ultrathin transferrable microring laser," *ACS Applied Materials & Interfaces*, Vol. 13, No. 16, 19 324–19 331, 2021.

[32] Xu, Z., Q. Hong, K. Ge, X. Shi, X. Wang, J. Deng, Z. Zhou, and T. Zhai, "Random lasing from label-free living cells for rapid cytometry of apoptosis," *Nano Letters*, Vol. 22, No. 1, 172–178, 2022.

[33] Lafargue, C., S. Bittner, S. Lozenko, J. Lautru, J. Zyss, C. Ulysse, C. Cluzel, and M. Lebental, "Three-dimensional emission from organic Fabry-Perot microlasers," *Applied Physics Letters*, Vol. 102, No. 25, 251120, 2013.

[34] Pan, J., Y. Yao, L. Yang, H. Li, and S. He, "Optically transparent and mechanically flexible coplanar waveguide-fed wideband antenna based on sub-micron thick micro-metallic meshes," *Progress In Electromagnetics Research*, Vol. 176, 11–23, 2022.

[35] De La Rue, R. M. and C. Seassal, "Photonic crystal devices: Some basics and selected topics," *Laser & Photonics Reviews*, Vol. 6, No. 4, 564–597, 2012.

[36] Zhai, T.-R., D.-H. Liu, and X.-D. Zhang, "Photonic crystals and microlasers fabricated with low refractive index material," *Frontiers of Physics in China*, Vol. 5, 266–276, 2010.

[37] Bendickson, J. M., J. P. Dowling, and M. Scalora, "Analytic expressions for the electromagnetic mode density in finite, one-dimensional, photonic band-gap structures," *Physical Review*

E, Vol. 53, No. 4, 4107, 1996.

[38] Boedecker, G. and C. Henkel, "All-frequency effective medium theory of a photonic crystal," *Optics Express*, Vol. 11, No. 13, 1590–1595, 2003.

[39] Wang, Z., T. Zhai, J. Lin, and D. Liu, "Effect of surface truncation on mode density in photonic crystals," *JOSA B*, Vol. 24, No. 9, 2416–2420, 2007.

[40] Painter, O., R. K. Lee, A. Scherer, A. Yariv, J. D. O'brien, P. D. Dapkus, and I. Kim, "Two-dimensional photonic band-gap defect mode laser," *Science*, Vol. 284, No. 5421, 1819–1821, 1999.

[41] Yang, X. and C. W. Wong, "Coupled-mode theory for stimulated Raman scattering in high-Q/Vm silicon photonic band gap defect cavity lasers," *Optics Express*, Vol. 15, No. 8, 4763–4780, 2007.

[42] Park, H.-G., S.-H. Kim, S.-H. Kwon, Y.-G. Ju, J.-K. Yang, J.-H. Baek, S.-B. Kim, and Y.-H. Lee, "Electrically driven single-cell photonic crystal laser," *Science*, Vol. 305, No. 5689, 1444–1447, 2004.

[43] Jung, H., M. Lee, C. Han, Y. Park, K.-S. Cho, and H. Jeon, "Efficient on-chip integration of a colloidal quantum dot photonic crystal band-edge laser with a coplanar waveguide," *Optics Express*, Vol. 25, No. 26, 32 919–32 930, 2017.

[44] Ryu, H.-Y., S.-H. Kwon, Y.-J. Lee, Y.-H. Lee, and J.-S. Kim, "Very-low-threshold photonic band-edge lasers from free-standing triangular photonic crystal slabs," *Applied Physics Letters*, Vol. 80, No. 19, 3476–3478, 2002.

[45] Monat, C., C. Seassal, X. Letartre, P. Regreny, P. Rojo-Romeo, P. Viktorovitch, M. L. V. d'Yerville, D. Cassagne, J. P. Albert, E. Jalaguier, S. Pocas, and B. Aspar, "InP-based two-dimensional photonic crystal on silicon: In-plane Bloch mode laser," *Applied Physics Letters*, Vol. 81, No. 27, 5102–5104, 2002.

[46] Imada, M., S. Noda, A. Chutinan, T. Tokuda, M. Murata, and G. Sasaki, "Coherent two-dimensional lasing action in surface-emitting laser with triangular-lattice photonic crystal structure," *Applied Physics Letters*, Vol. 75, No. 3, 316–318, 1999.

[47] Meier, M., A. Mekis, A. Dodabalapur, A. Timko, R. E. Slusher, J. D. Joannopoulos, and O. Nalamasu, "Laser action from two-dimensional distributed feedback in photonic crystals," *Applied Physics Letters*, Vol. 74, No. 1, 7–9, 1999.

[48] Fu, Y. and T. Zhai, "Distributed feedback organic lasing in photonic crystals," *Frontiers of Optoelectronics*, Vol. 13, 18–34, 2020.

[49] Kang, M., T. Liu, C. T. Chan, and M. Xiao, "Applications of bound states in the continuum in photonics," *Nature Reviews Physics*, Vol. 5, No. 11, 659–678, 2023.

[50] Vardeny, Z. V., A. Nahata, and A. Agrawal, "Optics of photonic quasicrystals," *Nature Photonics*, Vol. 7, No. 3, 177–187, 2013.

[51] Lin, Y., C. Browning, R. B. Timens, D. H. Geuzebroek, C. G. H. Roeloffzen, M. Hoekman, D. Geskus, R. M. Oldenbeuving, R. G. Heideman, and Y. Fan, "Characterization of hybrid InP-TriPleX photonic integrated tunable lasers based on silicon nitride (Si_3N_4/SiO_2) microring resonators for optical coherent system," *IEEE Photonics Journal*, Vol. 10, No. 3, 1–8, 2018.

[52] Xiao, Y.-F. and F. Vollmer, "Special issue on the 60th anniversary of the first laser — Series I: Microcavity photonics — From fundamentals to applications," *Light: Science & Applications*, Vol. 10, No. 1, 141, 2021.

[53] Zhang, Q., W. Tao, J. Huang, R. Xia, and J. Cabanillas-Gonzalez, "Toward electrically pumped organic lasers: A review and outlook on material developments and resonator architectures," *Advanced Photonics Research*, Vol. 2, No. 5, 2000155, 2021.

[54] Khurgin, J. B., "Exceptional points in polaritonic cavities and subthreshold Fabry-Perot lasers," *Optica*, Vol. 7, No. 8, 1015–1023, 2020.

[55] Zhang, Q., S.-W. Wang, X. Liu, T. Chen, H. Li, J. Liang, W. Zheng, R. Agarwal, W. Lu, and A. Pan, "Low threshold, single-mode laser based on individual CdS nanoribbons in dielectric DBR microcavity," *Nano Energy*, Vol. 30, 481–487, 2016.

[56] Mi, Y., Z. Liu, Q. Shang, X. Niu, J. Shi, S. Zhang, J. Chen, W. Du, Z. Wu, R. Wang, X. Qiu, X. Hu, Q. Zhang, T. Wu, and X. Liu, "Fabry-Pérot oscillation and room temperature lasing in perovskite cube-corner pyramid cavities," *Small*, Vol. 14, No. 9, 1703136, 2018.

[57] Zhang, S., T. Zhai, L. Cui, X. Shi, K. Ge, N. Liang, and A. Hayat, "Tunable WGM laser based on the polymer thermo-optic effect," *Polymers*, Vol. 13, No. 2, 205, 2021.

[58] Hayat, A., J. Tong, C. Chen, L. Niu, G. Aziz, T. Zhai, and X. Zhang, "Multi-wavelength colloidal quantum dot lasers in distributed feedback cavities," *Science China Information Sciences*, Vol. 63, 1–7, 2020.

[59] Zhou, P., L. Niu, A. Hayat, F. Cao, T. Zhai, and X. Zhang, "Operating characteristics of high-order distributed feedback polymer lasers," *Polymers*, Vol. 11, No. 2, 258, 2019.

[60] Cao, F., L. Niu, J. Tong, S. Li, A. Hayat, M. Wang, T. Zhai, and X. Zhang, "Hybrid lasing in a plasmonic cavity," *Optics Express*, Vol. 26, No. 10, 13 383–13 389, 2018.

[61] Chang, J.-F., M. C. Gwinner, M. Caironi, T. Sakanoue, and H. Sirringhaus, "Conjugated-polymer-based lateral heterostructures defined by high-resolution photolithography," *Advanced Functional Materials*, Vol. 20, No. 17, 2825–2832, 2010.

[62] Shkunov, M. N., Z. V. Vardeny, M. C. DeLong, R. C. Polson, A. A. Zakhidov, and R. H. Baughman, "Tunable, gap-state lasing in switchable directions for opal photonic crystals," *Advanced Functional Materials*, Vol. 12, No. 1, 21–26, 2002.

[63] Kok, M. H., W. Lu, W. Y. Tam, and G. K. L. Wong, "Lasing from dye-doped icosahedral quasicrystals in dichromate gelatin emulsions," *Optics Express*, Vol. 17, No. 9, 7275–7284, 2009.

[64] Zhang, W., J. Yao, and Y. S. Zhao, "Organic micro/nanoscale lasers," *Accounts of Chemical Research*, Vol. 49, No. 9, 1691–1700, 2016.

[65] Grivas, C. and M. Pollnau, "Organic solid-state integrated amplifiers and lasers," *Wiley Online Library*, 419–462, 2012.

[66] Song, L., L. Shen, and H. Wang, "Squeezing of hyperbolic polaritonic rays in cylindrical lamellar structures," *Progress In Electromagnetics Research*, Vol. 174, 23–32, 2022.

[67] Kavokin, A. V., J. J. Baumberg, G. Malpuech, and F. P. Laussy, *Microcavities*, Oxford University Press, 2017.

[68] Xiao, Y.-F. and Q. Gong, "Optical microcavity: From fundamental physics to functional photonics devices," *Science Bulletin*, Vol. 61, 185–186, 2016.

[69] Zhang, Q., Q. Shang, R. Su, T. T. H. Do, and Q. Xiong, "Halide perovskite semiconductor lasers: Materials, cavity design, and low threshold," *Nano Letters*, Vol. 21, No. 5, 1903–1914, 2021.

[70] Chénais, S. and S. Forget, "Recent advances in solid-state organic lasers," *Polymer International*, Vol. 61, No. 3, 390–406, 2012.

[71] Jiang, Y., Y.-Y. Liu, X. Liu, H. Lin, K. Gao, W.-Y. Lai, and W. Huang, "Organic solid-state lasers: A materials view and future development," *Chemical Society Reviews*, Vol. 49, No. 16, 5885–5944, 2020.

[72] Dai, J., C. Zhao, J. Xu, H. Roshan, H. Dong, F. D. Stasio, F. Yuan, B. Jiao, and Z. Wu, "Double hole transport layers deliver promising-performance in light-emitting diodes based on $MAPbBr_3$ nanocrystals," *Organic Electronics*, Vol. 124, 106941, 2024.

[73] Yan, R., D. Gargas, and P. Yang, "Nanowire photonics," *Nature Photonics*, Vol. 3, No. 10, 569–576, 2009.

[74] Clark, J. and G. Lanzani, "Organic photonics for communications," *Nature Photonics*, Vol. 4, No. 7, 438–446, 2010.

[75] Ziel, Van der J. P., W. T. Tsang, R. A. Logan, R. M. Mikulyak, and W. M. Augustyniak, "Subpicosecond pulses from passively mode-locked GaAs buried optical guide semiconductor lasers," *Applied Physics Letters*, Vol. 39, No. 7, 525–527, 1981.

[76] San Miguel, M., Q. Feng, and J. V. Moloney, "Light-polarization dynamics in surface-emitting semiconductor lasers," *Physical Review A*, Vol. 52, No. 2, 1728, 1995.

[77] Ledentsov, N. N., V. M. Ustinov, A. Y. Egorov, A. E. Zhukov, M. V. Maksimov, I. G. Tabatadze, and P. S. Kop'ev, "Optical properties of heterostructures with InGaAs-GaAs quantum clusters," *Semiconductors*, Vol. 28, No. 8, 832–834, 1994.

[78] Bimberg, D., M. Grundmann, F. Heinrichsdorff, N. N. Ledentsov, V. M. Ustinov, A. E. Zhukov, A. R. Kovsh, M. V. Maximov, Y. M. Shernyakov, B. V. Volovik, *et al.*, "Quantum dot lasers: Breakthrough in optoelectronics," *Thin Solid Films*, Vol. 367, No. 1-2, 235–249, 2000.

[79] Veldhuis, S. A., P. P. Boix, N. Yantara, M. Li, T. C. Sum, N. Mathews, and S. G. Mhaisalkar, "Perovskite materials for light-emitting diodes and lasers," *Advanced Materials*, Vol. 28, No. 32, 6804–6834, 2016.

[80] Tang, C. W. and S. A. VanSlyke, "Organic electroluminescent diodes," *Applied Physics Letters*, Vol. 51, No. 12, 913–915, 1987.

[81] Tessler, N., G. J. Denton, and R. H. Friend, "Lasing from conjugated-polymer microcavities," *Nature*, Vol. 382, No. 6593, 695–697, 1996.

[82] Goossens, M., A. Ruseckas, G. A. Turnbull, and I. D. W. Samuel, "Subpicosecond pulses from a gain-switched polymer distributed feedback laser," *Applied Physics Letters*, Vol. 85, No. 1, 31–33, 2004.

[83] Marcus, M., J. D. Milward, A. Köhler, and W. Barford, "Structural information for conjugated polymers from optical modeling," *The Journal of Physical Chemistry A*, Vol. 122, No. 14, 3621–3625, 2018.

[84] Giovanella, U., P. Betti, A. Bolognesi, S. Destri, M. Melucci, M. Pasini, W. Porzio, and C. Botta, "Core-type polyfluorene-based copolymers for low-cost light-emitting technologies," *Organic Electronics*, Vol. 11, No. 12, 2012–2018, 2010.

[85] Lawrence, J. R., G. A. Turnbull, I. D. W. Samuel, G. J. Richards, and P. L. Burn, "Optical amplification in a first-generation dendritic organic semiconductor," *Optics Letters*, Vol. 29, No. 8, 869–871, 2004.

[86] Spehr, T., A. Siebert, T. Fuhrmann-Lieker, J. Salbeck, T. Rabe, T. Riedl, H. H. Johannes, W. Kowalsky, J. Wang, T. Weimann, and P. Hinze, "Organic solid-state ultraviolet-laser based on spiro-terphenyl," *Applied Physics Letters*, Vol. 87, 161103, 2005.

[87] Zhai, T., Y. Wang, L. Chen, X. Wu, S. Li, and X. Zhang, "Red-green-blue laser emission from cascaded polymer membranes," *Nanoscale*, Vol. 7, No. 47, 19 935–19 939, 2015.

[88] Yap, B. K., R. Xia, M. Campoy-Quiles, P. N. Stavrinou, and D. D. C. Bradley, "Simultaneous optimization of charge-carrier mobility and optical gain in semiconducting polymer films," *Nature Materials*, Vol. 7, No. 5, 376–380, 2008.

[89] Sim, M., J. Shin, C. Shim, M. Kim, S. B. Jo, J.-H. Kim, and K. Cho, "Dependence of exciton diffusion length on crystalline order in conjugated polymers," *The Journal of Physical Chemistry C*, Vol. 118, No. 2, 760–766, 2014.

[90] Yan, M., L. J. Rothberg, F. Papadimitrakopoulos, M. E. Galvin, and T. M. Miller, "Spatially indirect excitons as primary photoexcitations in conjugated polymers," *Physical Review Letters*, Vol. 72, No. 7, 1104, 1994.

[91] Heliotis, G., D. D. C. Bradley, G. A. Turnbull, and I. D. W. Samuel, "Light amplification and gain in polyfluorene waveguides," *Applied Physics Letters*, Vol. 81, No. 3, 415–417, 2002.

[92] Chang, S.-J., X. Liu, T.-T. Lu, Y.-Y. Liu, J.-Q. Pan, Y. Jiang, S.-Q. Chu, W.-Y. Lai, and W. Huang, "Ladder-type poly(indenofluorene-co-benzothiadiazole)s as efficient gain media for organic lasers: Design, synthesis, optical gain properties, and stabilized lasing properties," *Journal of Materials Chemistry C*, Vol. 5, No. 26, 6629–6639, 2017.

[93] Vandyshev, Y. V., V. S. Dneprovskii, V. I. Klimov, and D. K. Okorokov, "Lasing on a transition between quantum-well levels in a quantum dot," *Jetp Lett.*, Vol. 54, No. 8, 442, 1991.

[94] Wu, H., X. Cheng, S. Xie, Y. Huang, R. A. Janjua, X. Liu, and S. He, "Aluminum quantum dots with surface controlled Blue-UV photoluminescence," *The Journal of Physical Chemistry C*, Vol. 127, No. 5, 2687–2693, 2023.

[95] Bae, W. K., L. A. Padilha, Y.-S. Park, H. McDaniel, I. Robel, J. M. Pietryga, and V. I. Klimov, "Controlled alloying of the core-shell interface in CdSe/CdS quantum dots for suppression of Auger recombination," *ACS Nano*, Vol. 7, No. 4, 3411–3419, 2013.

[96] Wu, K., Y.-S. Park, J. Lim, and V. I. Klimov, "Towards zero-threshold optical gain using charged semiconductor quantum dots," *Nature Nanotechnology*, Vol. 12, No. 12, 1140–1147, 2017.

[97] Roh, J., Y.-S. Park, J. Lim, and V. I. Klimov, "Optically pumped colloidal-quantum-dot lasing in LED-like devices with an integrated optical cavity," *Nature Communications*, Vol. 11, No. 1, 271, 2020.

[98] Lim, J., Y.-S. Park, and V. I. Klimov, "Optical gain in colloidal quantum dots achieved with direct-current electrical pumping," *Nature Materials*, Vol. 17, No. 1, 42–49, 2018.

[99] Kovalenko, M. V., L. Manna, A. Cabot, Z. Hens, D. V. Talapin, C. R. Kagan, V. I. Klimov, A. L. Rogach, P. Reiss, D. J. Milliron, *et al.*, "Prospects of nanoscience with nanocrystals," *ACS Nano*, Vol. 9, No. 2, 1012–1057, 2015.

[100] Geiregat, P., D. Van Thourhout, and Z. Hens, "A bright future for colloidal quantum dot lasers," *NPG Asia Materials*, Vol. 11, No. 1, 41, 2019.

[101] Klimov, V. I., "Mechanisms for photogeneration and recombination of multiexcitons in semiconductor nanocrystals: Implications for lasing and solar energy conversion," *The Journal of Physical Chemistry B*, Vol. 110, No. 34, 16 827–16 845, 2006.

[102] Pietryga, J. M., Y.-S. Park, J. Lim, *et al.*, "Spectroscopic and device aspects of nanocrystal quantum dots," *Chemical Reviews*, Vol. 116, No. 18, 10 513–10 622, 2016.

[103] Kondo, T., T. Azuma, T. Yuasa, and R. Ito, "Biexciton lasing in the layered perovskite-type material (C6H13NH3) 2PbI4," *Solid State Communications*, Vol. 105, No. 4, 253–255, 1998.

[104] Xing, G., N. Mathews, S. S. Lim, N. Yantara, X. Liu, D. Sabba, M. Grätzel, S. Mhaisalkar, and T. C. Sum, "Low-temperature solution-processed wavelength-tunable perovskites for lasing," *Nature Materials*, Vol. 13, No. 5, 476–480, 2014.

[105] Zhang, Q., R. Su, W. Du, X. Liu, L. Zhao, S. T. Ha, and Q. Xiong, "Advances in small perovskite-based lasers," *Small*

Methods, Vol. 1, No. 9, 1700163, 2017.

[106] Zhao, F., A. Ren, P. Li, Y. Li, J. Wu, and Z. M. Wang, "Toward continuous-wave pumped metal halide perovskite lasers: Strategies and challenges," *ACS Nano*, Vol. 16, No. 5, 7116–7143, 2022.

[107] Wang, K., S. Wang, S. Xiao, and Q. Song, "Recent advances in perovskite micro- and nanolasers," *Advanced Optical Materials*, Vol. 6, No. 18, 1800278, 2018.

[108] Protesescu, L., S. Yakunin, M. I. Bodnarchuk, F. Krieg, R. Caputo, C. H. Hendon, R. X. Yang, A. Walsh, and M. V. Kovalenko, "Nanocrystals of cesium lead halide perovskites (CsPbX3, X = Cl, Br, and I): Novel optoelectronic materials showing bright emission with wide color gamut," *Nano Letters*, Vol. 15, No. 6, 3692–3696, 2015.

[109] Khmelevskaia, D., D. Markina, P. Tonkaev, M. Masharin, A. Peltek, P. Talianov, M. A. Baranov, A. Nikolaeva, M. V. Zyuzin, L. E. Zelenkov, *et al.*, "Excitonic versus free-carrier contributions to the nonlinearly excited photoluminescence in $CsPbBr_3$ perovskites," *ACS Photonics*, Vol. 9, No. 1, 179–189, 2021.

[110] Kim, J., S.-H. Lee, J. H. Lee, and K.-H. Hong, "The role of intrinsic defects in methylammonium lead iodide perovskite," *The Journal of Physical Chemistry Letters*, Vol. 5, No. 8, 1312–1317, 2014.

[111] Stranks, S. D., V. M. Burlakov, T. Leijtens, J. M. Ball, A. Goriely, and H. J. Snaith, "Recombination kinetics in organic-inorganic perovskites: Excitons, free charge, and subgap states," *Physical Review Applied*, Vol. 2, No. 3, 034007, 2014.

[112] Allegro, I., Y. Li, B. S. Richards, U. W. Paetzold, U. Lemmer, and I. A. Howard, "Bimolecular and auger recombination in phase-stable perovskite thin films from cryogenic to room temperature and their effect on the amplified spontaneous emission threshold," *The Journal of Physical Chemistry Letters*, Vol. 12, No. 9, 2293–2298, 2021.

[113] Cao, J., A. V. Kavokin, and A. V. Nalitov, "Tamm states and gap topological numbers in photonic crystals," *Progress In Electromagnetics Research*, Vol. 173, 141–149, 2022.

[114] Liao, T.-H., L. Tsang, S. Tan, and X. Xu, "Broadband Green's function-Multiple Scattering Theory for fast band solutions of vector electromagnetic waves in 3D perioidc strutures," in *2023 IEEE International Symposium on Antennas and Propagation and USNC-URSI Radio Science Meeting (USNC-URSI)*, 811–812, 2023.

[115] Zheng, J., Z. Guo, Y. Sun, H. Jiang, Y. Li, and H. Chen, "Topological edge modes in one-dimensional photonic artificial structures (Invited)," *Progress In Electromagnetics Research*, Vol. 177, 1–20, 2023.

[116] Mahmood, R., A. V. Ramirez, and A. C. Hillier, "Creating two-dimensional quasicrystal, supercell, and Moiré lattices with laser interference lithography: Implications for photonic bandgap materials," *ACS Applied Nano Materials*, Vol. 4, No. 9, 8851–8862, 2021.

[117] Chu, S., A. Hayat, F. Cao, and T. Zhai, "Single-mode lasing in polymer circular gratings," *Materials*, Vol. 14, No. 9, 2318, 2021.

[118] Kogelnik, H. and C. V. Shank, "Coupled-wave theory of distributed feedback lasers," *Journal of Applied Physics*, Vol. 43, No. 5, 2327–2335, 1972.

[119] Kazarinov, R. and C. Henry, "Second-order distributed feedback lasers with mode selection provided by first-order radiation losses," *IEEE Journal of Quantum Electronics*, Vol. 21, No. 2, 144–150, 1985.

[120] Zhai, T., X. Wu, M. Wang, F. Tong, S. Li, Y. Ma, J. Deng, and X. Zhang, "Dual-wavelength polymer laser based on an active/inactive/active sandwich-like structure," *Applied Physics Letters*, Vol. 109, No. 10, 101 906.1–101 906.3, 2016.

[121] Huang, W., S. Shen, D. Pu, G. Wei, Y. Ye, C. Peng, and L. Chen, "Working characteristics of external distributed feedback polymer lasers with varying waveguiding structures," *Journal of Physics D: Applied Physics*, Vol. 48, No. 49, 495105, 2015.

[122] Riechel, S., C. Kallinger, U. Lemmer, J. Feldmann, A. Gombert, V. Wittwer, and U. Scherf, "A nearly diffraction limited surface emitting conjugated polymer laser utilizing a two-dimensional photonic band structure," *Applied Physics Letters*, Vol. 77, No. 15, 2310–2312, 2000.

[123] Turnbull, G. A., P. Andrew, W. L. Barnes, and I. D. W. Samuel, "Photonic mode dispersion of a two-dimensional distributed feedback polymer laser," *Physical Review B*, Vol. 67, No. 16, 165107, 2003.

[124] Notomi, M., H. Suzuki, and T. Tamamura, "Directional lasing oscillation of two-dimensional organic photonic crystal lasers at several photonic band gaps," *Applied Physics Letters*, Vol. 78, No. 10, 1325–1327, 2001.

[125] Heliotis, G., R. Xia, D. D. C. Bradley, G. A. Turnbull, I. D. W. Samuel, P. Andrew, and W. L. Barnes, "Blue, surface-emitting, distributed feedback polyfluorene lasers," *Applied Physics Letters*, Vol. 83, No. 11, 2118–2120, 2003.

[126] Jung, H., C. Han, H. Kim, K.-S. Cho, Y.-G. Roh, Y. Park, and H. Jeon, "Tunable colloidal quantum dot distributed feedback lasers integrated on a continuously chirped surface grating," *Nanoscale*, Vol. 10, No. 48, 22 745–22 749, 2018.

[127] Zhai, T., X. Wu, F. Tong, S. Li, M. Wang, and X. Zhang, "Multi-wavelength lasing in a beat structure," *Applied Physics Letters*, Vol. 109, 261906, 2016.

[128] Karnutsch, C., C. Pflumm, G. Heliotis, J. C. Demello, D. D. C. Bradley, J. Wang, T. Weimann, V. Haug, C. Gärtner, and U. Lemmer, "Improved organic semiconductor lasers based on a mixed-order distributed feedback resonator design," *Applied Physics Letters*, Vol. 90, 131104, 2007.

[129] Bonal, V., J. M. Villalvilla, J. A. Quintana, *et al.*, "Blue and deep-blue-emitting organic lasers with top-layer distributed feedback resonators," *Advanced Optical Materials*, Vol. 8, No. 24, 2001153, 2020.

[130] Muñoz-Mármol, R., V. Bonal, G. M. Paternò, *et al.*, "Dual amplified spontaneous emission and lasing from nanographene films," *Nanomaterials*, Vol. 10, No. 8, 1525, 2020.

[131] Palatnik, A., C. Cho, C. Zhang, M. Sudzius, M. Kroll, S. Meister, and K. Leo, "Control of emission characteristics of perovskite lasers through optical feedback," *Advanced Photonics Research*, Vol. 2, No. 12, 2100177, 2021.

[132] Dong, Q., X. Fu, D. Seyitliyev, K. Darabi, J. Mendes, L. Lei, Y.-A. Chen, C.-H. Chang, A. Amassian, K. Gundogdu, *et al.*, "Cavity engineering of perovskite distributed feedback lasers," *ACS Photonics*, Vol. 9, No. 9, 3124–3133, 2022.

[133] Liu, F., T. Yin, Y. Liu, I. Naeem, D. Guo, L. Cui, and T. Zhai, "Multiple-beam colloidal quantum dot lasers in a waveguide-grating-waveguide microcavity," *Applied Physics Letters*, Vol. 123, No. 7, 071 105–1–7, 2023.

[134] Liu, Y., M. Liu, J. Hu, J. Li, and X. Zhang, "Mechanically contacted distributed-feedback optical microcavity," *Nanomaterials*, Vol. 12, No. 11, 1883, 2022.

[135] Zhang, L., C. Liao, B. Lv, X. Wang, M. Xiao, R. Xu, Y. Yuan, C. Lu, Y. Cui, and J. Zhang, "Single-mode lasing from "Giant" CdSe/CdS core-shell quantum dots in distributed feedback structures," *ACS Applied Materials & Interfaces*, Vol. 9, No. 15,

13 293–13 303, 2017.

[136] Harwell, J. R., G. L. Whitworth, G. A. Turnbull, and I. D. W. Samuel, "Green perovskite distributed feedback lasers," *Scientific Reports*, Vol. 7, No. 1, 11727, 2017.

[137] Ma, S., M. Wei, S. K. Rajendran, M. Karl, B. Xu, M. C. Gather, W. Tian, G. A. Turnbull, and I. D. W. Samuel, "Pick and place distributed feedback lasers using organic single crystals," *Advanced Optical Materials*, Vol. 8, No. 8, 1901785, 2020.

[138] Navarro-Fuster, V., I. Vragovic, E. M. Calzado, P. G. Boj, J. A. Quintana, J. M. Villalvilla, A. Retolaza, A. Juarros, D. Otaduy, S. Merino, and M. A. Díaz-García, "Film thickness and grating depth variation in organic second-order distributed feedback lasers," *Journal of Applied Physics*, Vol. 112, No. 4, 043 104–1–12, 2012.

[139] Aftenieva, O., M. Sudzius, A. Prudnikau, M. Adnan, S. Sarkar, V. Lesnyak, K. Leo, A. Fery, and T. A. König, "Lasing by template-assisted self-assembled quantum dots," *Advanced Optical Materials*, Vol. 11, No. 6, 2202226, 2023.

[140] Yuyama, S., T. Nakajima, K. Yamashita, and K. Oe, "Solid state organic laser emission at 970 nm from dye-doped fluorinated-polyimide planar waveguides," *Applied Physics Letters*, Vol. 93, No. 2, 023 306–1–3, 2008.

[141] Klinkhammer, S., T. Woggon, U. Geyer, C. Vannahme, S. Dehm, T. Mappes, and U. Lemmer, "A continuously tunable low-threshold organic semiconductor distributed feedback laser fabricated by rotating shadow mask evaporation," *Applied Physics B*, Vol. 97, 787–791, 2009.

[142] Roh, K., L. Zhao, and B. P. Rand, "Tuning laser threshold within the large optical gain bandwidth of halide perovskite thin films," *ACS Photonics*, Vol. 8, No. 8, 2548–2554, 2021.

[143] Zhai, T., L. Han, X. Ma, and X. Wang, "Low-threshold microlasers based on holographic dual-gratings," *Nanomaterials*, Vol. 11, No. 6, 1530, 2021.

[144] Jäckle, M., H. Linnenbank, M. Hentschel, M. Saliba, S. G. Tikhodeev, and H. Giessen, "Tunable green lasing from circular grating distributed feedback based on $CH_3NH_3PbBr_3$ perovskite," *Optical Materials Express*, Vol. 9, No. 5, 2006–2021, 2019.

[145] Guo, R., M. Nečada, T. K. Hakala, A. I. Väkeväinen, and P. Törmä, "Lasing at K points of a honeycomb plasmonic lattice," *Physical Review Letters*, Vol. 122, No. 1, 013901, 2019.

[146] Senevirathne, C. A. M., A. S. D. Sandanayaka, B. S. B. Karunathilaka, T. Fujihara, F. Bencheikh, C. Qin, K. Goushi, T. Matsushima, and C. Adachi, "Markedly improved performance of optically pumped organic lasers with two-dimensional distributed-feedback gratings," *ACS Photonics*, Vol. 8, No. 5, 1324–1334, 2021.

[147] Goldberg, I., N. Annavarapu, S. Leitner, K. Elkhouly, F. Han, N. Verellen, T. Kuna, W. Qiu, C. Rolin, J. Genoe, R. Gehlhaar, and P. Heremans, "Multimode lasing in all-solution-processed UV-nanoimprinted distributed feedback $MAPbI_3$ perovskite waveguides," *ACS Photonics*, Vol. 10, No. 5, 1591–1600, 2023.

[148] Fan, F., O. Voznyy, R. P. Sabatini, K. T. Bicanic, M. M. Adachi, J. R. McBride, K. R. Reid, Y.-S. Park, X. Li, A. Jain, *et al.*, "Continuous-wave lasing in colloidal quantum dot solids enabled by facet-selective epitaxy," *Nature*, Vol. 544, No. 7648, 75–79, 2017.

[149] Heliotis, G., R. Xia, G. A. Turnbull, P. Andrew, W. L. Barnes, I. D. W. Samuel, and D. D. C. Bradley, "Emission characteristics and performance comparison of polyfluorene lasers with one- and two-dimensional distributed feedback," *Advanced Functional Materials*, Vol. 14, No. 1, 91–97, 2004.

[150] Zhai, T., F. Tong, Y. Wang, X. Wu, S. Li, M. Wang, and X. Zhang, "Polymer lasers assembled by suspending membranes on a distributed feedback grating," *Optics Express*, Vol. 24, No. 19, 22 028–22 033, 2016.

[151] Zhai, T., Y. Wang, L. Chen, and X. Zhang, "Direct writing of tunable multi-wavelength polymer lasers on a flexible substrate," *Nanoscale*, Vol. 7, No. 29, 12 312–12 317, 2015.

[152] Zhai, T., F. Cao, S. Chu, Q. Gong, and X. Zhang, "Continuously tunable distributed feedback polymer laser," *Optics Express*, Vol. 26, No. 4, 4491–4497, 2018.

[153] Stellinga, D., M. E. Pietrzyk, J. M. E. Glackin, Y. Wang, A. K. Bansal, G. A. Turnbull, K. Dholakia, I. D. W. Samuel, and T. F. Krauss, "An organic vortex laser," *ACS Nano*, Vol. 12, No. 3, 2389–2394, 2018.

[154] Zhang, S., L.-B. Cui, X. Zhang, J.-H. Tong, and T. Zhai, "Tunable polymer lasing in chirped cavities," *Optics Express*, Vol. 28, No. 3, 2809–2817, 2020.

[155] Turnbull, G. A., P. Andrew, W. L. Barnes, and I. D. W. Samuel, "Operating characteristics of a semiconducting polymer laser pumped by a microchip laser," *Applied Physics Letters*, Vol. 82, No. 3, 313–315, 2003.

[156] Huang, W., D. Pu, W. Qiao, W. Wan, Y. Liu, Y. Ye, S. Wu, and L. Chen, "Tunable multi-wavelength polymer laser based on a triangular-lattice photonic crystal structure," *Journal of Physics D: Applied Physics*, Vol. 49, No. 33, 335103, 2016.

[157] Gao, Y., L. Y. M. Tobing, A. Kiffer, D. H. Zhang, C. Dang, and H. V. Demir, "Azimuthally polarized, circular colloidal quantum dot laser beam enabled by a concentric grating," *ACS Photonics*, Vol. 3, No. 12, 2255–2261, 2016.

[158] Prins, F., D. K. Kim, J. Cui, E. D. Leo, L. L. Spiegel, K. M. McPeak, and D. J. Norris, "Direct patterning of colloidal quantum-dot thin films for enhanced and spectrally selective out-coupling of emission," *Nano Letters*, Vol. 17, No. 3, 1319–1325, 2017.

[159] Sun, W., Y. Liu, G. Qu, Y. Fan, W. Dai, Y. Wang, Q. Song, J. Han, and S. Xiao, "Lead halide perovskite vortex microlasers," *Nature Communications*, Vol. 11, No. 1, 4862, 2020.

[160] Koshelev, K., G. Favraud, A. Bogdanov, Y. Kivshar, and A. Fratalocchi, "Nonradiating photonics with resonant dielectric nanostructures," *Nanophotonics*, Vol. 8, No. 5, 725–745, 2019.

[161] Hwang, M.-S., J.-H. Choi, K.-Y. Jeong, K.-H. Kim, H.-R. Kim, J.-P. So, H.-C. Lee, J. Kim, S.-H. Kwon, and H.-G. Park, "Recent advances in nanocavities and their applications," *Chemical Communications*, Vol. 57, No. 40, 4875–4885, 2021.

[162] Von Neumann, J. and E. P. Wigner, "Über merkwürdige diskrete eigenwerte," *The Collected Works of Eugene Paul Wigner: Part A: The Scientific Papers*, 291–293, 1993.

[163] Azzam, S. I. and A. V. Kildishev, "Photonic bound states in the continuum: From basics to applications," *Advanced Optical Materials*, Vol. 9, No. 1, 2001469, 2021.

[164] Hwang, M.-S., K.-Y. Jeong, J.-P. So, K.-H. Kim, and H.-G. Park, "Nanophotonic nonlinear and laser devices exploiting bound states in the continuum," *Communications Physics*, Vol. 5, No. 1, 106, 2022.

[165] Marinica, D. C., A. G. Borisov, and S. V. Shabanov, "Bound states in the continuum in photonics," *Physical Review Letters*, Vol. 100, No. 18, 183902, 2008.

[166] Hsu, C. W. and B. Zhen, "A. D. stone, JD joannopoulos, and M. soljacic," *Nat. Rev. Mater*, Vol. 1, 16048, 2016.

[167] Yang, Y., C. Peng, Y. Liang, Z. Li, and S. Noda, "Analytical perspective for bound states in the continuum in photonic crystal slabs," *Physical Review Letters*, Vol. 113, No. 3, 037401,

2014.

[168] Rivera, N., C. W. Hsu, B. Zhen, H. Buljan, J. D. Joannopoulos, and M. Soljačić, "Controlling directionality and dimensionality of radiation by perturbing separable bound states in the continuum," *Scientific Reports*, Vol. 6, No. 1, 33394, 2016.

[169] Liu, V., M. Povinelli, and S. Fan, "Resonance-enhanced optical forces between coupled photonic crystal slabs," *Optics Express*, Vol. 17, No. 24, 21 897–21 909, 2009.

[170] Lepetit, T., E. Akmansoy, J.-P. Ganne, and J.-M. Lourtioz, "Resonance continuum coupling in high-permittivity dielectric metamaterials," *Physical Review B*, Vol. 82, No. 19, 195307, 2010.

[171] Wu, M., L. Ding, R. P. Sabatini, L. K. Sagar, G. Bappi, R. Paniagua-Domínguez, E. H. Sargent, and A. I. Kuznetsov, "Bound state in the continuum in nanoantenna-coupled slab waveguide enables low-threshold quantum-dot lasing," *Nano Letters*, Vol. 21, No. 22, 9754–9760, 2021.

[172] Wang, Y., Y. Fan, X. Zhang, H. Tang, Q. Song, J. Han, and S. Xiao, "Highly controllable etchless perovskite microlasers based on bound states in the continuum," *ACS Nano*, Vol. 15, No. 4, 7386–7391, 2021.

[173] Song, Q. H. and H. Cao, "Improving optical confinement in nanostructures via external mode coupling," *Physical Review Letters*, Vol. 105, No. 5, 053902, 2010.

[174] Hirose, K., Y. Liang, Y. Kurosaka, A. Watanabe, T. Sugiyama, and S. Noda, "Watt-class high-power, high-beam-quality photonic-crystal lasers," *Nature Photonics*, Vol. 8, No. 5, 406–411, 2014.

[175] Hsu, C. W., B. Zhen, J. Lee, S.-L. Chua, S. G. Johnson, J. D. Joannopoulos, and M. Soljačić, "Observation of trapped light within the radiation continuum," *Nature*, Vol. 499, No. 7457, 188–191, 2013.

[176] Jin, J., X. Yin, L. Ni, M. Soljačić, B. Zhen, and C. Peng, "Topologically enabled ultrahigh-Q guided resonances robust to out-of-plane scattering," *Nature*, Vol. 574, No. 7779, 501–504, 2019.

[177] Hwang, M.-S., H.-C. Lee, K.-H. Kim, K.-Y. Jeong, S.-H. Kwon, K. Koshelev, Y. Kivshar, and H.-G. Park, "Ultralow-threshold laser using super-bound states in the continuum," *Nature Communications*, Vol. 12, No. 1, 4135, 2021.

[178] Ha, S. T., Y. H. Fu, N. K. Emani, Z. Pan, R. M. Bakker, R. Paniagua-Domínguez, and A. I. Kuznetsov, "Directional lasing in resonant semiconductor nanoantenna arrays," *Nature Nanotechnology*, Vol. 13, No. 11, 1042–1047, 2018.

[179] Ha, S. T., R. Paniagua-Domínguez, and A. I. Kuznetsov, "Room-temperature multi-beam, multi-wavelength bound states in the continuum laser," *Advanced Optical Materials*, Vol. 10, No. 19, 2200753, 2022.

[180] Huang, Z.-T., C.-Y. Chang, K.-P. Chen, and T.-C. Lu, "Tunable lasing direction in one-dimensional suspended high-contrast grating using bound states in the continuum," *Advanced Photonics*, Vol. 4, No. 6, 066004, 2022.

[181] Tan, M. J. H., J.-E. Park, F. Freire-Fernández, J. Guan, X. G. Juarez, and T. W. Odom, "Lasing action from quasi-propagating modes," *Advanced Materials*, Vol. 34, No. 34, 2203999, 2022.

[182] Chen, M.-H., D. Xing, V.-C. Su, Y.-C. Lee, Y.-L. Ho, and J.-J. Delaunay, "Gan ultraviolet laser based on bound states in the continuum (BIC)," *Advanced Optical Materials*, Vol. 11, No. 6, 2201906, 2023.

[183] Kodigala, A., T. Lepetit, Q. Gu, B. Bahari, Y. Fainman, and B. Kanté, "Lasing action from photonic bound states in continuum," *Nature*, Vol. 541, No. 7636, 196–199, 2017.

[184] Wu, M., S. T. Ha, S. Shendre, E. G. Durmusoglu, W.-K. Koh, D. R. Abujetas, J. A. Sánchez-Gil, R. Paniagua-Domínguez, H. V. Demir, and A. I. Kuznetsov, "Room-temperature lasing in colloidal nanoplatelets via Mie-resonant bound states in the continuum," *Nano Letters*, Vol. 20, No. 8, 6005–6011, 2020.

[185] Ren, Y., P. Li, Z. Liu, Z. Chen, Y.-L. Chen, C. Peng, and J. Liu, "Low-threshold nanolasers based on miniaturized bound states in the continuum," *Science Advances*, Vol. 8, No. 51, eade8817, 2022.

[186] Zhong, H., Y. Yu, Z. Zheng, Z. Ding, X. Zhao, J. Yang, Y. Wei, Y. Chen, and S. Yu, "Ultra-low threshold continuous-wave quantum dot mini-BIC lasers," *Light: Science & Applications*, Vol. 12, No. 1, 100, 2023.

[187] Bahari, B., F. Vallini, T. Lepetit, R. Tellez-Limon, J. H. Park, A. Kodigala, Y. Fainman, and B. Kante, "Integrated and steerable vortex lasers using bound states in continuum," *arXiv preprint arXiv:1707.00181*, 2017.

[188] Huang, C., C. Zhang, S. Xiao, Y. Wang, Y. Fan, Y. Liu, N. Zhang, G. Qu, H. Ji, J. Han, *et al.*, "Ultrafast control of vortex microlasers," *Science*, Vol. 367, No. 6481, 1018–1021, 2020.

[189] Zhang, X., Y. Liu, J. Han, Y. Kivshar, and Q. Song, "Chiral emission from resonant metasurfaces," *Science*, Vol. 377, No. 6611, 1215–1218, 2022.

[190] Tian, J., G. Adamo, H. Liu, M. Wu, M. Klein, J. Deng, N. S. S. Ang, R. Paniagua-Domínguez, H. Liu, A. I. Kuznetsov, and C. Soci, "Phase-change perovskite microlaser with tunable polarization vortex," *Advanced Materials*, Vol. 35, No. 1, 2207430, 2023.

[191] Tang, R., Y. Shi, H. Shang, J. Wu, H. Ma, M. Wei, Y. Luo, Z. Chen, Y. Ye, J. Jian, *et al.*, "Two-dimensional heterostructure quasi-BIC photonic crystal surface-emitting laser with low divergence," *Nanophotonics*, Vol. 12, No. 16, 3257–3265, 2023.

[192] Sinelnik, A. D., I. I. Shishkin, X. Yu, K. B. Samusev, P. A. Belov, M. F. Limonov, P. Ginzburg, and M. V. Rybin, "Experimental observation of intrinsic light localization in photonic icosahedral quasicrystals," *Advanced Optical Materials*, Vol. 8, No. 21, 2001170, 2020.

[193] Cheng, W., W. Liu, Q. Liu, and F. Chen, "Observation of topological anderson phase in laser-written quasi-periodic waveguide arrays," *Optics Letters*, Vol. 47, No. 11, 2883–2886, 2022.

[194] Cheng, Z., R. Savit, and R. Merlin, "Structure and electronic properties of thue-morse lattices," *Physical Review B*, Vol. 37, No. 9, 4375, 1988.

[195] Dulea, M., M. Johansson, and R. Riklund, "Localization of electrons and electromagnetic waves in a deterministic aperiodic system," *Physical Review B*, Vol. 45, No. 1, 105, 1992.

[196] Levine, D. and P. J. Steinhardt, "Quasicrystals: A new class of ordered structures," *Physical Review Letters*, Vol. 53, No. 26, 2477, 1984.

[197] Shechtman, D., I. Blech, D. Gratias, and J. W. Cahn, "Metallic phase with long-range orientational order and no translational symmetry," *Physical Review Letters*, Vol. 53, No. 20, 1951, 1984.

[198] Kohmoto, M., B. Sutherland, and K. Iguchi, "Localization of optics: Quasiperiodic media," *Physical Review Letters*, Vol. 58, No. 23, 2436, 1987.

[199] Matsui, T., A. Agrawal, A. Nahata, and Z. V. Vardeny, "Transmission resonances through aperiodic arrays of subwavelength apertures," *Nature*, Vol. 446, No. 7135, 517–521, 2007.

[200] Zoorob, M. E., M. D. B. Charlton, G. J. Parker, J. J. Baumberg, and M. C. Netti, "Complete photonic bandgaps in 12-fold symmetric quasicrystals," *Nature*, Vol. 404, No. 6779, 740–743, 2000.

[201] Boxer, M., M. Mazloumi, P. Snell, P. Rochon, and R. G. Sabat, "Large-area photonic crystals, quasicrystals, and Moiré quasicrystals fabricated on azobenzene molecular glass films by pyramidal interference lithography," *Optical Materials Express*, Vol. 12, No. 11, 4362–4374, 2022.

[202] Gumbs, G. and M. K. Ali, "Dynamical maps, Cantor spectra, and localization for Fibonacci and related quasiperiodic lattices," *Physical Review Letters*, Vol. 60, No. 11, 1081, 1988.

[203] Hattori, T., N. Tsurumachi, S. Kawato, and H. Nakatsuka, "Photonic dispersion relation in a one-dimensional quasicrystal," *Physical Review B*, Vol. 50, No. 6, 4220, 1994.

[204] Werchner, M., M. Schafer, M. Kira, S. W. Koch, J. Sweet, J. D. Olitzky, J. Hendrickson, B. C. Richards, G. Khitrova, H. M. Gibbs, *et al.*, "One dimensional resonant Fibonacci quasicrystals: Noncanonical linear and canonical nonlinear effects," *Optics Express*, Vol. 17, No. 8, 6813–6828, 2009.

[205] Janot, C. and P. Paufler, "Quasicrystals: A primer," *Crystal Research and Technology*, Vol. 31, No. 6, 738–738, 1996.

[206] Sutherland, B. and M. Kohmoto, "Resistance of a one-dimensional quasicrystal: Power-law growth," *Physical Review B*, Vol. 36, No. 11, 5877, 1987.

[207] Poddubny, A. N., L. Pilozzi, M. M. Voronov, and E. L. Ivchenko, "Resonant Fibonacci quantum well structures in one dimension," *Physical Review B*, Vol. 77, No. 11, 113306, 2008.

[208] Notomi, M., H. Suzuki, T. Tamamura, and K. Edagawa, "Lasing action due to the two-dimensional quasiperiodicity of photonic quasicrystals with a Penrose lattice," *Physical Review Letters*, Vol. 92, No. 12, 123906, 2004.

[209] Mahler, L., A. Tredicucci, F. Beltram, C. Walther, J. Faist, H. E. Beere, D. A. Ritchie, and D. S. Wiersma, "Quasi-periodic distributed feedback laser," *Nature Photonics*, Vol. 4, No. 3, 165–169, 2010.

[210] Hayat, A., L. Cui, H. Liang, S. Zhang, M. A. Khan, G. Aziz, and T. Zhai, "Colloidal quantum dots lasing and coupling in 2D holographic photonic quasicrystals," *Optics Express*, Vol. 29, No. 10, 15 145–15 158, 2021.

[211] Nozaki, K. and T. Baba, "Quasiperiodic photonic crystal microcavity lasers," *Applied Physics Letters*, Vol. 84, No. 24, 4875–4877, 2004.

[212] Nozaki, K. and T. Baba, "Lasing characteristics of 12-fold symmetric quasi-periodic photonic crystal slab nanolasers," *Japanese Journal of Applied Physics*, Vol. 45, No. 8R, 6087, 2006.

[213] Cui, L., A. Hayat, L. Lv, Z. Xu, and T. Zhai, "A theoretical model of quasicrystal resonators: A guided optimization approach," *Crystals*, Vol. 11, No. 7, 749, 2021.

[214] Luo, D., Q. G. Du, H. T. Dai, X. H. Zhang, and X. W. Sun, "Temperature effect on lasing from penrose photonic quasicrystal," *Optical Materials Express*, Vol. 4, No. 6, 1172–1177, 2014.

[215] Biasco, S., A. Ciavatti, L. Li, A. G. Davies, E. H. Linfield, H. Beere, D. Ritchie, and M. S. Vitiello, "Highly efficient surface-emitting semiconductor lasers exploiting quasicrystalline distributed feedback photonic patterns," *Light: Science & Applications*, Vol. 9, No. 1, 54, 2020.

[216] Yang, G., X. Chen, Y. Wang, and S. Feng, "Lasing characteristic of organic octagonal quasicrystal slabs with single-defect microcavity at low-index contrast," *Optics Express*, Vol. 21, No. 9, 11 457–11 464, 2013.

[217] Cai, Y., X. Jiao, X. Chen, X. Wang, S. Feng, Z. Wang, and Y. Wang, "Low threshold optically pumped lasing from MEH-PPV quasi-periodic photonic crystal microcavity," *Applied Optics*, Vol. 58, No. 18, 4853–4857, 2019.

[218] Lee, P.-T., T.-W. Lu, F.-M. Tsai, T.-C. Lu, and H.-C. Kuo, "Whispering gallery mode of modified octagonal quasiperiodic photonic crystal single-defect microcavity and its side-mode reduction," *Applied Physics Letters*, Vol. 88, No. 20, 201 104–1–20, 2006.

[219] Li, M. S., A. Y.-G. Fuh, and S.-T. Wu, "Multimode lasing from the microcavity of an octagonal quasi-crystal based on holographic polymer-dispersed liquid crystals," *Optics Letters*, Vol. 37, No. 15, 3249–3251, 2012.

[220] Luo, D., Y. Li, X. W. Xu, and Q. G. Du, "Lasing from organic quasicrystal fabricated by seven- and nine-beam interference," *Optics Express*, Vol. 24, No. 11, 12 330–12 335, 2016.

[221] Hong, K.-B., C.-C. Chen, T.-C. Lu, and S.-C. Wang, "Lasing characteristics of GaN-based photonic quasi-crystal surface emitting lasers operated at higher order Γ mode," *IEEE Journal of Selected Topics in Quantum Electronics*, Vol. 21, No. 6, 743–748, 2015.

[222] Ren, J., X. Sun, and S. Wang, "A low threshold nanocavity in a two-dimensional 12-fold photonic quasicrystal," *Optics & Laser Technology*, Vol. 101, 42–48, 2018.

[223] Biasco, S., A. Ciavatti, L. Li, A. G. Davies, E. H. Linfield, H. Beere, D. Ritchie, and M. S. Vitiello, "Highly efficient surface-emitting semiconductor lasers exploiting quasicrystalline distributed feedback photonic patterns," *Light: Science & Applications*, Vol. 9, No. 1, 1498–1508, 2020.

[224] Cai, Y., S. Zhang, C. Wu, Z. Wang, W. Xu, X. Chen, and Y. Wang, "Octagonal quasicrystal defect mode laser-based PVK: Ir(ppy)3 polymer driven by optical pumping," *Nanomaterials*, Vol. 12, No. 9, 1386, 2022.

[225] Liu, Z., D. Luo, Q. Du, Y. Li, and H. Dai, "Emission characteristics of lasing from all organic mirrorless quasicrystal," *IEEE Photonics Journal*, Vol. 8, No. 6, 1–6, 2016.

[226] Li, Y., Q. Du, Z. Liu, R. Chen, H. Dai, and D. Luo, "Pump angle and position effects on laser emission from quasicrystal microcavity by nine-beam interference based on holographic polymer-dispersed liquid crystals," *Liquid Crystals*, Vol. 45, No. 3, 415–420, 2018.

[227] Liu, Z., R. Chen, Y. Liu, X. Zhang, X. Sun, W. Huang, and D. Luo, "Low-threshold, single-mode, and linearly polarized lasing from all organic quasicrystal microcavity," *Optics Express*, Vol. 25, No. 18, 21 519–21 525, 2017.

[228] Luo, D., Q. G. Du, H. T. Dai, H. V. Demir, H. Z. Yang, W. Ji, and X. W. Sun, "Strongly linearly polarized low threshold lasing of all organic photonic quasicrystals," *Scientific Reports*, Vol. 2, No. 1, 627, 2012.

[229] Zah, C.-E., M. R. Amersfoort, B. N. Pathak, F. J. Favire, P. S. D. Lin, N. C. Andreadakis, A. W. Rajhel, R. Bhat, C. Caneau, M. A. Koza, *et al.*, "Multiwavelength DFB laser arrays with integrated combiner and optical amplifier for WDM optical networks," *IEEE Journal of Selected Topics in Quantum Electronics*, Vol. 3, No. 2, 584–597, 1997.

[230] Arai, S., N. Nishiyama, T. Maruyama, and T. Okumura, "GaInAsP/InP membrane lasers for optical interconnects," *IEEE Journal of Selected Topics in Quantum Electronics*, Vol. 17, No. 5, 1381–1389, 2011.

[231] Watanabe, T., Y. Saijo, Y. Hasegawa, K. Watanabe, Y. Nishijima, and T. Baba, "Ion-sensitive photonic-crystal nanolaser sensors," *Optics Express*, Vol. 25, No. 20, 24 469–24 479, 2017.

[232] Saadatmand, S. B., V. Ahmadi, and S. M. Hamidi, "Quasi-BIC based all-dielectric metasurfaces for ultra-sensitive refractive index and temperature sensing," *Scientific Reports*, Vol. 13, No. 1, 20625, 2023.

[233] Kao, T. S., Y. T. Lo, and H.-C. Kuo, "Imaging functions of quasi-periodic nanohole array as an ultra-thin planar optical lens," in *Photonics*, Vol. 2, No. 2, 619–633, 2015.

[234] Zhang, F., C. Wang, K. Yin, X. R. Dong, Y. X. Song, Y. X. Tian, and J. A. Duan, "Quasi-periodic concave microlens array for liquid refractive index sensing fabricated by femtosecond laser assisted with chemical etching," *Scientific Reports*, Vol. 8, No. 1, 2419, 2018.

[235] Retolaza, A., J. Martinez-Perdiguero, S. Merino, M. Morales-Vidal, P. G. Boj, *et al.*, "Organic distributed feedback laser for label-free biosensing of $ErbB_2$ protein biomarker," *Sensors and Actuators B: Chemical*, Vol. 223, 261–265, 2016.

[236] Du, Y., N. Liu, X. Wu, K. Liu, and J. Li, "Frequency division multiplexing and wavelength stabilized 2f/1f wavelength modulation spectroscopy for simultaneous trace CH_4 and CO_2 detection," *Spectrochimica Acta Part A: Molecular and Biomolecular Spectroscopy*, Vol. 305, 123453, 2023.

[237] Li, F., T. Zhang, G. Wang, and S. He, "Simultaneous detection of CO_2 and N_2O based on quartz-enhanced photothermal spectroscopy by using NIR and MIR lasers," *Progress In Electromagnetics Research M*, Vol. 118, 137–149, 2023.

[238] Sano, T., R. Losakul, and H. Schmidt, "Dual optofluidic distributed feedback dye lasers for multiplexed biosensing applications," *Scientific Reports*, Vol. 13, No. 1, 16824, 2023.

[239] Buckley, B. B., S. T. M. Fryslie, K. Guinn, G. Morrison, A. Gazman, Y. Shen, K. Bergman, M. L. Mashanovitch, and L. A. Johansson, "WDM source based on high-power, efficient 1280-nm DFB lasers for terabit interconnect technologies," *IEEE Photonics Technology Letters*, Vol. 30, No. 22, 1929–1932, 2018.

[240] Liu, X., F. Li, Y. Li, T. Tang, Y. Liao, Y. Lu, and Q. Wen, "Terahertz metasurfaces based on bound states in the continuum (BIC) for high-sensitivity refractive index sensing," *Optik*, Vol. 261, 169248, 2022.

[241] Di, W., T. Wang, X. Gao, H. Wang, Q. Fang, C. Qian, H. Qian, H. Chen, and T. Wang, "Quasi-BIC lasing at Telecom wavelengths and its potential application in biosensing," *IEEE Sensors Journal*, Vol. 24, No. 1, 238–245, 2024.

[242] Zhang, H., T. Wang, J. Tian, J. Sun, S. Li, I. D. Leon, R. P. Zaccaria, L. Peng, F. Gao, X. Lin, H. Chen, and G. Wang, "Quasi-BIC laser enabled by high-contrast grating resonator for gas detection," *Nanophotonics*, Vol. 11, No. 2, 297–304, 2021.

[243] Xu, D., J. Ding, and L. Peng, "Structured illumination imaging with quasi-periodic patterns," *Journal of Biophotonics*, Vol. 13, No. 6, e201960209, 2020.